1 **Long chain diols in settling particles in tropical oceans:**

2 **insights into sources, seasonality and proxies.**

4 Marijke W. de Bar*[,1], Jenny E. Ullgren[2], Robert C. Thunnell[‡], Stuart G. Wakeham[3], Geert-Jan

5 A. Brummer[4,5], Jan-Berend W. Stuut[4,5], Jaap S. Sinninghe Damsté[1,6] and Stefan Schouten[1,6]

7 [1] NIOZ Royal Netherlands Institute for Sea Research, Department of Marine Microbiology

8 and Biogeochemistry, and Utrecht University, P.O. Box 59, 1790 AB Den Burg, Texel, the

9 Netherlands

10 [2] Runde Miljøsenter, Runde, Norway

11 [3] Skidaway Institute of Oceanography, University of Georgia, 10 Ocean Science Circle,

12 Savannah, USA

13 [4] NIOZ Royal Netherlands Institute for Sea Research, Department of Ocean Systems, and

14 Utrecht University, P.O. Box 59, 1790 AB Den Burg, Texel, the Netherlands

15 [5] Vrije Universiteit Amsterdam, Faculty of Science, Department of Earth Sciences, De

16 Boelelaan 1085, 1081HV Amsterdam, the Netherlands

17 [6] Department of Earth Sciences, Faculty of Geosciences, Utrecht University, the Netherlands

19 * Corresponding author: Marijke W. de Bar (Marijke.de.Bar@nioz.nl)

[‡] Deceased: 30 July 2018.

ABSTRACT

In this study we have analyzed sediment trap time series from five tropical sites to assess seasonal variations in concentrations and fluxes of long-chain diols (LCDs) and associated proxies with emphasis on the Long chain Diol Index (LDI) temperature proxy. For the tropical Atlantic, we observe that generally less than 2 % of LCDs settling from the water column are preserved in the sediment. The Atlantic and Mozambique Channel traps reveal minimal seasonal variations in the LDI, similar to the two other lipid-based temperature proxies TEX_{86} and $U^{K'}_{37}$. In addition, annual mean LDI-derived temperatures are in good agreement with the annual mean satellite-derived sea surface temperatures (SSTs). In contrast, the LDI in the Cariaco Basin shows larger seasonal variation, as do the TEX_{86} and $U^{K'}_{37}$. Here, the LDI underestimates SST during the warmest months, which is likely due to summer stratification and the habitat depth of the diol producers deepening to around 20 to 30 m. Surface sediment LDI temperatures in the Atlantic and Mozambique Channel compare well with the average LDI-derived temperatures from the overlying sediment traps, as well as with decadal annual mean SST. Lastly, we observed large seasonal variations in the Diol Index, as indicator of upwelling conditions, at three sites: in the Eastern Atlantic potentially linked to Guinea Dome upwelling, in the Cariaco Basin likely caused by seasonal upwelling, and in the Mozambique Channel where Diol Index variations may be driven by upwelling from favorable winds and/or eddy migration.

1. Introduction

Several proxies exist for the reconstruction of past sea surface temperature (SST) based on lipids. The $U^{K'}_{37}$ is one of the most applied proxies and is based on the unsaturation of long-chain alkenones (LCAs), which are produced by phototrophic haptophyte algae, mainly the cosmopolitan *Emiliania huxleyi* (Volkman et al., 1980; Brassell et al., 1986; Prahl and Wakeham, 1987; Conte et al., 1994). This index exhibits a strong positive correlation with SST (Müller et al., 1998; Conte et al., 2006). Another widely used organic paleotemperature proxy is the TEX_{86}, as originally proposed by Schouten et al. (2002), based on the relative distribution of archaeal membrane lipids, i.e. glycerol dialkyl glycerol tetraethers (GDGTs), and in the marine realm are mainly thought to be derived from the phylum Thaumarchaeota. Schouten et al. (2002) showed that the TEX_{86} index measured in marine surface sediments is correlated with SST, and since then its application in paleoenvironmental studies has increased (see e.g. review by Tierney, 2014). However, research showed that despite their highest abundance being recorded in the upper 100 m of the water column, Thaumarchaeota can be present down to 5000 m depth (Karner et al., 2001; Herndl et al., 2005). Accordingly, GDGTs may be found in high concentrations below 100 m depth (e.g., Sinninghe Damsté et al., 2002; Wuchter et al., 2005) and several studies have indicated that TEX_{86} might be more reflective of subsurface temperatures in some regions (e.g., Huguet et al., 2007; Lopes dos Santos et al., 2010; Kim et al., 2012; 2015; Schouten et al., 2013; Chen et al., 2014; Tierney et al., 2017; see Zhang and Liu, 2018 for review).

Most recently a SST proxy based on the distribution of long-chain diols (LCDs), called the Long-chain Diol Index, or LDI was proposed (Rampen et al., 2012). This index is a ratio of 1,13- and 1,15-diols (i.e., alcohol groups at position C-1 and C-13 or C-15), and the analysis of globally distributed surface sediments revealed that this index strongly correlates with SST. Since then, the index has been applied in several paleoenvironmental studies (e.g., Naafs et al., 2012; Lopes dos Santos et al., 2013; Jonas et al., 2017; Warnock et al., 2017). However, large gaps still remain in the understanding of this proxy. The largest uncertainty is that the main marine producer of LCDs is unknown. Although these diols have been observed in cultures of certain marine eustigmatophyte algae (e.g. Volkman et al., 1992; 1999; Méjanelle et al., 2003; Rampen et al., 2014b), the LCD distributions in cultures are different from those

observed in marine sediments. Furthermore, Balzano et al. (2018) combined lipid analyses with 18S rRNA gene amplicon sequencing on suspended particulate matter (SPM) and did not find a significant direct correlation between LCD concentrations and sequences of known LCD-producers. Rampen et al. (2012) observed the strongest empirical relation between surface sediment derived LDI values and SSTs for autumn and summer, suggesting that these are the main growth seasons of the source organisms. Moreover, the strongest correlation was also observed for the upper 20 m of the water column, suggesting that the LCDs are likely produced by phototrophic algae which thrive in the euphotic zone. Nevertheless, LDI-temperatures based on surface sediments reflect an integrated signal of many years, which complicates the interpretation of the LDI in terms of seasonal production and depth of export production.

One way of resolving seasonality in LCD flux and LDI is to analyze time series samples from sediment traps that continuously collect sinking particles in successive time intervals over periods of a year or more. Such studies have been carried out for the $U^{K'}_{37}$ as well as for the TEX_{86} and associated lipids (e.g., Müller and Fischer, 2001; Wuchter et al., 2006; Huguet et al., 2007; Fallet et al., 2011; Yamamoto et al., 2012; Rosell-Melé and Prahl, 2013; Türich et al., 2013). However, very few studies have been done for LCDs. Villanueva et al. (2014) carried out a sediment trap study in Lake Challa (East Africa) and Rampen et al. (2008) in the upwelling region off Somalia. The latter study showed that 1,14-diols, produced by *Proboscia* diatoms strongly increased early in the upwelling season in contrast to 1,13- and 1,15-diols and thus can be used to trace upwelling. However, neither of these sediment trap studies have evaluated the LDI.

In this study, we assess seasonal patterns of the LDI for sediment trap series at five sites, i.e., in the Cariaco Basin, the Mozambique Channel and three sites in the tropical North Atlantic and compared the LDI values to satellite-derived SST, as well as results obtained for other temperature proxies, i.e. the TEX^{H}_{86} and $U^{K'}_{37.}$ Moreover, for the Atlantic and Mozambique Channel, we compare the sediment trap proxy signals with those preserved in the underlying sediments, after settling and burial. Finally, we assess the applicability of the Diol Index, based on 1,14-diols produced by *Proboscia* diatoms (Sinninghe Damsté et al., 2003), as tracer of upwelling and/or productivity in these regions.

2. Materials and methods

2.1 Study sites and sample collection

2.1.1   Tropical North Atlantic

The ocean current and wind patterns of the tropical Atlantic are mostly determined by the seasonal latitudinal shift of the intertropical convergence zone (ITCZ; Figure 1). The ITCZ migrates southward during boreal winter, and northward during boreal summer. During summer, the south-east trade winds prevail, whereas during winter the north-east trade winds intensify. The north-east trade winds drive the North Equatorial Current (NEC) which flows westward. South of the NEC, the North Equatorial Countercurrent (NECC) flows towards the east (Stramma and Schott, 1999). The South Equatorial Current (SEC) flows westward and branches off in the north Brazil Current (NBC; Stramma and Schott, 1999). When the ITCZ is in the north, the NBC retroflects off the South American coast, and is carried eastward into the NECC, and thus into the western tropical Atlantic (e.g., Richardson and Reverdin, 1987). North of the NBC, the Guiana Current (GC) disperses the outflow from the Amazon River towards the Caribbean Sea. (Müller-Karger et al., 1988; 1995). However, during boreal summer the NBC may retroflect, carrying the Amazon River plume far into the western Atlantic (e.g., Lefèvre et al., 1998; Müller-Karger et al., 1998; Coles et al., 2013). In fact, every late summer/autumn, the Amazon River outflow covers around 2×10^6 km^2 of the western North Atlantic, and the river delivers approximately half of all freshwater input into the tropical Atlantic (see Araujo et al., 2017 and references therein).

The eastern tropical North Atlantic is characterized by upwelling caused by the interaction between the trade winds and the movement of the ITCZ. Cropper et al. (2014) measured upwelling intensity along the NW African coastline between 1981 and 2012, in terms of wind speed, SST and other meteorological data. They recognized three latitudinal zones: weak permanent annual upwelling north of 26° N, strong permanent upwelling between 21° and 26° N and seasonal upwelling between 12° and 19° N related to the seasonal migration of the trade winds. Southeast of Cape Verde, large-scale cyclonic circulation forms the Guinea Dome (GD; Fig. 1), which centers around 10° N,22° W (Mazeika, 1967), i.e., close to mooring site M1. The GD is a thermal upwelling dome, formed by near-surface flow fields associated

121 with the westward NEC, the eastward NECC and the westward North Equatorial Undercurrent (NEUC)

122 (Siedler et al., 1992). It forms a cyclonic circulation as a result of the eastward flowing NECC and the

123 westward flowing NEC (Rossignol and Meyrueis, 1964; Mazeika, 1967). The GD develops from late

124 spring to late fall due to the northward ITCZ position and the resulting Ekman upwelling, but shows

125 significant interannual variability (Siedler et al., 1992; Yamagata and Iizuka, 1995; Doi et al., 2009)

126 judging from general ocean circulation models. According to Siedler et al. (1992), upwelling is most

127 intense between July and October when the ITCZ is in the GD region and the NECC is strongest.

128 At three sites, we analyzed five sediment trap series along a longitudinal transect in the North Atlantic

129 (~12° N) to determine seasonal variations in the LDI. This transect has been studied previously for

130 Saharan dust deposition in terms of grain sizes (van der Does et al., 2016), as the tropical North Atlantic

131 receives approximately one third of the wind-blown Saharan dust (e.g., Duce et al., 1991; Stuut et al.,

132 2005), which might potentially act as fertilizer because of the high iron levels (e.g., Martin and

133 Fitzwater, 1988; Korte et al., 2017; Guirreiro et al., 2017; Goudie and Middleton, 2001 and references

134 therein). Furthermore, Korte et al. (2017) assessed mass fluxes and mineralogical composition,

135 Guerreiro et al. (2017) measured coccolith fluxes for two of the time series, while Schreuder et al.

136 (2018a; 2018b) measured long-chain n-alkanes, long-chain n-alkanols and fatty acids, and levoglucosan

137 for the same sediment trap samples and surface sediments as analyzed in this study.

138 At site M1 (12.00° N, 23.00° W), the sediment trap, referred to as M1U, was moored at a water depth

139 of 1150 m (Fig. 1). This mooring is located in the proximity of the Guinea Dome, and might therefore

140 potentially be influenced by seasonal upwelling. At station M2 (13.81° N, 37.82° W), two sediment

141 traps were recovered, i.e., an 'upper' (M2U) trap at a water depth of 1235 m, and a 'lower' (M2L) trap

142 at a depth of 3490 m. Lastly, at mooring station M4 (12.06° N, 49.19° W), also an upper and lower trap

143 series were recovered and analyzed (M4U and M4L), at 1130 and 3370 m depth, respectively. This

144 mooring site may seasonally be affected by Amazon River discharge (van der Does et al., 2016; Korte

145 et al., 2017; Guirreiro et al., 2017; Schreuder et al., 2018a). All sediment traps were equipped with 24

146 sampling cups, which sampled synchronously over 16-day intervals from October 2012 to November

147   2013, using $HgCl_2$ as a biocide and borax as a pH buffer to prevent in situ decomposition of the collected

148   material.

149

150   **2.1.2   Mozambique Channel**

151   The Mozambique Channel is located between Madagascar and Mozambique and is part of the Agulhas

152   Current system hugging the coast of South Africa (Lutjeharms, 2006). The Agulhas Current system is

153   an important conveyor in the transport of warm and salty waters from the Indian to the Atlantic Ocean

154   (Gordon, 1986; Weijer et al., 1999; Peeters et al., 2004). The northern part of the channel is also

155   influenced by the East African monsoon winds (Biastoch and Krauss, 1999; Sætre and da Silva, 1982;

156   Malauene et al., 2014). Between September and March, these winds blow from the northeast, parallel

157   to the Mozambique coastline, favoring coastal upwelling. Additionally, the Mozambique Channel is

158   largely influenced by fast-rotating, mesoscale eddies which migrate southward towards the Agulhas

159   region. Using satellite altimetry, Schouten et al. (2003) observed on average 4 to 6 eddies, ca. 300 km

160   in diameter, propagating yearly from the central Mozambique Channel (15° S) toward the Agulhas area

161   (35° S) between 1995 and 2000. Seasonal upwelling occurs off Northern Mozambique (between ca. 15

162   and 18° S) (Nehring et al., 1987; Malauene et al., 2014), from August to March with a dominant period

163   of about two months although periods of one to four weeks have also been observed (Malauene et al.,

164   2014).

165   The sediment trap was moored at 16.8° S and 40.8° E, at a water depth of 2250 m (Fig. 1; Fallet et al.,

166   2010, 2011) and of the same type as used for the North Atlantic transect. We analyzed the LCD proxies

167   for two respective time intervals: the first interval covers ca. 3.5 years, from November 2003 to

168   September 2007, with a sampling interval of 21 days. The second interval covers another year, between

169   February 2008 and February 2009, with a sampling interval of 17 days. Previously, Fallet et al. (2011)

170   published foraminiferal, $U^{K'}_{37}$ and TEX_{86} records for the first time interval, and the organic carbon

171   content for the follow-up time series. For further details on the deployments and sample treatments, we

172   refer to Fallet et al. (2011, 2012). The two surface sediments are located across the narrowest transect

173   between Mozambique and Madagascar, and were analyzed for $U^{K'}_{37}$ and TEX_{86} by Fallet et al. (2012)

174   and for LCDs by Lattaud et al. (2017b).

175

2.1.3   Cariaco Basin

177   The Cariaco Basin is one of the largest marine anoxic basins (Richards, 1975), located on the continental

178   shelf of Venezuela. The basin is characterized by permanent stratification and strongly influenced by

179   the migration of the intertropical convergence zone (ITCZ). During late autumn and winter, the ITCZ

180   migrates to the south which results in decreased precipitation and trade wind intensification which in

181   turn induces upwelling and surface water cooling. This seasonal upwelling is a major source of nutrients

182   that leads to strong phytoplankton growth along the Venezuelan coast (e.g., Müller-Karger et al., 2001;

183   Thunell et al., 2007). Between August and October, the ITCZ moves northward again, resulting in a

184   rainy season and diminishing of the trade winds inhibiting upwelling. During this wet season the

185   contribution of terrestrially derived nutrients is higher. Due to the prevalent anoxic conditions in the

186   basin, there is no bioturbation which has resulted in the accumulation of laminated sediments which

187   provide excellent annually to decadally resolved climate records (e.g., Peterson et al., 1991; Hughen et

188   al., 1996; 1998). Moreover, in November 1995, a time series experiment started to facilitate research on

189   the link between biogeochemistry and the downward flux of particulate material under anoxic and

190   upwelling   conditions   (Thunell   et   al.,   2000).   This   project   (CARIACO;

191   http://imars.marine.usf.edu/cariaco) involved hydrographic cruises (monthly), water column chemistry

192   measurements and sediment trap sampling (every 14 days). One mooring containing four automated

193   sediment traps (Honjo and Doherty, 1988) was deployed at $10.50°$ N and $64.67°$ W, at a bottom depth

194   of around 1400 m. These traps were moored at 275 m depth, just above the oxic/anoxic interface (Trap

195   A), 455 m (Trap B), 930 m (Trap C) and 1255 m (Trap D). All traps contain a 13-cup carousel which

196   collected sinking particles over 2 weeks, and were serviced every half year. For further details on trap

197   deployment and recovery, and sample collection, storage and processing we refer to Thunell et al. (2000)

198   and Goñi et al. (2004). In addition to the sediment trap sampling, the primary productivity of the surface

199   waters was measured every month using ^{14}C incubations (Müller-Karger et al., 2001; 2004). For this

study, we investigated two periods, i.e., May 1999–May 2000 and July 2002–July 2003 for Traps A and B. These years include upwelling and non-upwelling periods, as well as a disastrous flooding event in December 1999 (Turich et al., 2013). Turich et al. (2013) identified the upwelling periods, linked to the migration of the ITCZ, as indicated by decreasing SST in the CTD (temperature at -1 m water depth) and satellite-based measurements (indicated by grey boxes in figures 8 and 10), and shoaling of the average depths of primary production and increased primary production. Moreover, Turich et al. (2013) evaluated the $U^{K'}_{37}$ and TEX_{86} proxies for the same two time series for which we analyzed the LCD proxies.

2.2 Instrumental data

Satellite SST, precipitation and wind speed time series of the M1, M2 and M4 moorings in the Atlantic derive from Guerreiro et al. (2017 and in revision) who retrieved these data from the Ocean Biology Processing Group (OBPG, 2014) (Frouin et al., 2003), the Goddard Earth Sciences Data and Information Services Center (2016) (Huffman et al., 2007; Xie and Arkin, 1997) and NASA Aquarius project (2015a; 2015b) (Lee et al., 2012) (see supplement of Guerreiro et al., 2017 for detailed references). The SST and Chlorophyll *a* time series data for the Mozambique Channel were adapted from Fallet et al. (2011), who retrieved these data from the Giovanni database (for details see Fallet et al., 2011). Surface sediment proxy temperatures were compared to annual mean SST estimates derived from the World Ocean Atlas (2013) (decadal averages from 1955 to 2012; Locarnini et al., 2013). Sea surface temperature data for the Cariaco Basin were adopted from Turich et al. (2013) and combined with additional CTD temperatures from the CARIACO time series data base for the depths of 2, 5, 10, 15 and 20 m (http://www.imars.usf.edu/CAR/index.html.; CARIACO time series composite CTD profiles; lead principal investigator: Frank Müller-Karger).

    2.3 Lipid extraction

225   **2.3.1 Tropical North Atlantic**

226   The 120 sediment trap samples were sieved through a 1 mm mesh wet-split into five aliquots (van der

227   Does et al., 2016), of which one was washed with Milli-Q water, freeze-dried and homogenized for

228   chemical analysis (Korte et al., 2017). For organic geochemistry, sub-aliquots (by weight) were

229   extracted as described by Schreuder et al. (2018a). Shortly, ca. 100 mg dry weight of sediment trap

230   residue, and between 1.5 and 10 g of dry weight of surface sediment were extracted by ultrasonication

231   using a mixture of dichloromethane:methanol (DCM:MeOH) (2:1; v/v), and dried over a Na_2SO_4

232   column. For quantification of LCDs, LCAs and GDGTs, we added the following internal standards to

233   the total lipid extracts (TLEs): 2.04 µg C_{22} 7,16-diol (Rodrigo-Gamiz et al., 2015), 1.50 µg 10-

234   nonadecanone ($C_{19:0}$ ketone) and 0.1 µg C_{46} GDGT (Huguet et al., 2006), respectively. Subsequently,

235   the TLEs were separated into apolar (containing *n*-alkanes), ketone (containing LCAs) and polar

236   (containing LCDs and GDGTs) fractions over an activated (2h at 150 °C) Al_2O_3 column by eluting with

237   hexane/DCM (9:1; v/v), hexane/DCM (1:1; v/v) and DCM/MeOH (1:1; v/v), respectively. The apolar

238   fractions were analyzed by Schreuder et al. (2018a) for *n*-alkanes. Polar fractions were split for GDGT

239   (25 %) and LCD (75 %) analysis. The LCD fraction was silylated by the addition of BSTFA (*N*,*O*-

240   bis(trimethylsilyl)trifluoroacetamide) and pyridine, and heating at 60 °C for 20 min, after which ethyl

241   acetate was added prior to analysis. The ketone fraction was also dissolved in ethyl acetate, and analyzed

242   by GC and GC/MS. The GDGT fraction was dissolved in hexane:isopropanol (99:1, v/v), filtered

243   through a 0.45 μm polytetrafluoroethylene (PTFE) filter and analyzed by HPLC-MS.

244

245   **2.3.2 Mozambique Channel**

246   Aliquots of the sediment trap samples from the Mozambique Channel were previously extracted and

247   analyzed by Fallet et al. (2011) and Fallet et al. (2012), respectively. The sediment trap material was

248   extracted by ultrasonication using a mixture of DCM/MeOH (2:1; v/v), dried over Na_2SO_4, and

249   separated into apolar, ketone and polar fractions via alumina pipette column chromatography, by eluting

250   with hexane/DCM (9:1; v/v), hexane/DCM (1:1; v/v) and DCM/MeOH (1:1; v/v), respectively. These

existing polar fractions of the sediment trap material were silylated (as described above), dissolved in ethyl acetate and re-analyzed for LCDs by GC-MS. Since no record was kept of the aliquoting of extracts and polar fractions, we report the results in relative abundance rather than concentrations and fluxes of diols.

2.3.3 Cariaco Basin

Sediment trap material was extracted as described by Turich et al. (2013). Briefly, 1/16 aliquots of the trap samples were extracted by means of Bligh-Dyer extraction with sonication using a phosphate buffer and a trichloroacetic acid (TCA) buffer, after which the extracts were separated by adding 5 % NaCl in solvent-extracted distilled deionized water, and the organic phase was collected and the aqueous phase was extracted two more times. The extracts were pooled and dried over Na_2SO_4 and separated by means of Al_2O_3 column chromatography, eluting with hexane:DCM (9:1; v/v), DCM:MeOH (1:1; v/v) and MeOH. For this study, the DCM:MeOH (1:1; v/v) fraction was silylated (as described above), dissolved in ethyl acetate, and analyzed for LCDs using GC-MS. Similar to the Mozambique Channel samples, no record was kept of the aliquoting of extracts and polar fractions, and thus we report the results in relative abundance.

2.4   Instrumental analysis

2.4.1 GDGTs

The GDGT fractions of the surface sediments and sediment traps SPM samples of the tropical North Atlantic were analyzed for GDGTs by means of Ultra High Performance Liquid Chromatography Mass Spectrometry (UHPLC-MS). We used an Agilent 1260 HPLC, which is equipped with an automatic injector, interfaced with a 6130 Agilent MSD, and HP Chemstation software according to Hopmans et al. (2016). Compound separation was achieved by 2 silica BEH HILIC columns in tandem (150 mm x 2.1 mm; 1.7 µm; Waters Acquity) in normal phase, at 25 °C. GDGTs were eluted isocratically for 25 min with 18 % B, followed by a linear gradient to 35 % B in 25 minutes and finally a linear gradient to 100 % B in the last 30 min. A = hexane; B = hexane:isopropanol (9:1; v/v). The flow rate was constant at 0.2 mL min^{-1}, and the injection volume was 10 µL. The APCI-MS conditions are described by

278   Hopmans et al. (2016). Detection and quantification of GDGTs was achieved in single ion monitoring

279   (SIM) mode of the protonated molecules ($[M+H]^+$) of the GDGTs. We used a mixture of crenarchaeol

280   and the C_{46} GDGT (internal standard) to assess the relative response factor, which was used for

281   quantification of the GDGTs in the samples (c.f. Huguet et al., 2006).

282   Sea surface temperatures were calculated by means of the TEX^H_{86} as defined by Kim et al. (2010), which

283   is a logarithmic function of the original TEX_{86} index (Schouten et al., 2002):

284    $$\mathrm{TEX}^{H}_{86} = \log \frac{[GDGT-2] + [GDGT-3] + [Cren']}{[GDGT-1] + [GDGT-2] + [GDGT-3] + [Cren']} \qquad [1]$$

285   where the numbers indicate the number of cyclopentane moieties of the isoprenoid GDGTs, and *Cren´*

286   reflects an isomer of crenarchaeol, i.e. containing a cyclopentane moiety with a *cis* stereochemistry

287   (Sinninghe Damsté et al., 2018). The TEX^H_{86} values were translated to SSTs using the core-top

288   calibration of Kim et al. (2010):

289    $$\mathrm{SST} = 68.4 \times \mathrm{TEX}^{H}_{86} + 38.6 \qquad [2]$$

290   The Branched Isoprenoid Tetraether (BIT) index is a proxy for the relative contribution of terrestrial

291   derived organic carbon (Hopmans et al., 2004). We have calculated the modified version as reported by

292   de Jonge et al. (2014; 2015) which is based on the original index as proposed by Hopmans et al. (2004),

293   but includes the 6-methyl brGDGTs:

294    $$\mathrm{BIT} = \frac{[brGDGT\ Ia] + [brGDGT\ IIa+IIa'] + [brGDGT\ IIIa+IIIa']}{[brGDGT\ Ia] + [brGDGT\ IIa+IIa'] + [brGDGT\ IIIa+IIIa'] + [Cren]} \qquad [3]$$

295   where the numbers reflect different branched GDGTs (see Hopmans et al., 2004) and *Cren* reflects

296   crenarchaeol. The branched GDGTs were always around the detection limit in the Atlantic samples,

297   implying a BIT index of around zero and thus minimal influence of soil organic carbon (Hopmans et al.,

298   2004), and thus the BIT index is not discussed any further.

299

2.4.2 LCAs

The ketone fractions of the surface sediments and sediment traps samples of the tropical North Atlantic were analyzed for LCAs on an Agilent 6890N gas chromatograph (GC) with flame ionization detection (FID) after dissolving in ethyl acetate. The GC was equipped with a fused silica column with a length of 50 m, a diameter of 0.32 mm, and a coating of CP Sil-5 (film thickness = 0.12 μm). Helium was used as carrier gas, and the flow mode was a constant pressure of 100 kPa. The ketone fractions were injected on-column at a starting temperature of 70 °C, which increased by 20 °C min^{-1} to 200 °C followed by 3 °C min^{-1} until the final temperature of 320 °C was reached. This end temperature was held for 25 min.

The $U^{K'}_{37}$ index was calculated according to Prahl and Wakeham (1987):

$$U^{K'}_{37} = \frac{[C_{37:2}]}{[C_{37:2}] + [C_{37:3}]} \qquad [4]$$

The $U^{K'}_{37}$ values were translated to SST after the calibration of Müller et al. (1998):

$$SST = \frac{U^{K'}_{37} - 0.044}{0.033} \qquad [5]$$

We have also applied the recently proposed BAYSPLINE Bayesian calibration of Tierney and Tingley (2018). They and others have shown that the $U^{K'}_{37}$ estimates substantially attenuate above temperatures of 24 °C (e.g., Conte et al., 1998; Goñi et al., 2001; Sicre et al., 2002). The Bayesian calibration moves the upper limit of the $U^{K'}_{37}$ calibration from approximately 28 to 29.6 °C at unity. Since our traps are located in tropical regions with SSTs > 24 °C, we have applied this calibration as well.

2.4.3 LCDs

The silylated polar fractions were injected on-column on an Agilent 7890B GC coupled to an Agilent 5977A MS. The starting temperature was 70 °C, and increased to 130 °C by 20 °C min^{-1}, followed by a linear gradient of 4 °C min^{-1} to an end temperature of 320 °C, which was held for 25 min. 1μL was injected, and separation was achieved on a fused silica column (25 × 0.32 mm) coated with CP Sil-5 (film thickness 0.12 μm). Helium was used as carrier gas with a constant flow of 2 mL min^{-1}. The MS

operated with an ionization energy of 70 eV. Identification of LCDs was done in full scan mode, scanning between m/z 50–850, based on characteristic fragmentation patterns (Volkman et al., 1992; Versteegh et al., 1997). Proxy calculations and LCD quantifications were performed by analysis in SIM mode of the characteristic fragments (m/z 299, 313, 327 and 341; Rampen et al., 2012; m/z 187 for internal diol standard). For quantification of LCDs in the sediment traps and seafloor sediments of the tropical Atlantic, the peak areas of the LCDs were corrected for the average relative contribution of the selected SIM fragments to the total ion counts, i.e., 16 % for the saturated LCDs, 9 % for unsaturated LCDs and 25 % for the C_{22} 7,16-diol internal standard.

Sea surface temperatures were calculated using the LDI, according to Rampen et al. (2012):

$$\text{LDI} = \frac{[C_{30}\ 1,15-diol]}{[C_{28}\ 1,13-diol] + [C_{30}\ 1,13-diol] + [C_{30}\ 1,15-diol]} \quad [6]$$

These LDI values were converted into SSTs using the following equation (Rampen et al., 2012):

$$\text{SST} = \frac{\text{LDI} - 0.095}{0.033} \quad [7]$$

Upwelling conditions were reconstructed using the Diol Index as proposed by Rampen et al. (2008):

$$\text{Diol Index} = \frac{[C_{28}\ 1,14-diol] + [C_{30}\ 1,14-diol]}{[C_{28}\ 1,14-diol] + [C_{30}\ 1,14-diol] + [C_{30}\ 1,15-diol]} \quad [8]$$

In 2010, Willmott et al. introduced an alternative Diol Index, which is defined as the ratio of 1,14-diols over 1,13-diols. Since the index of Rampen et al. (2008) includes the C_{30} 1,15-diol, it can be affected by temperature variation, and therefore we would normally prefer to use the index of Willmott et al. (2010). However, we often did not detect the C_{28} 1,13-diol, or it co-eluted with cholest-5-en-7-one-3β-ol, compromising the calculation of the Diol Index of Willmott et al. (2010). Moreover, the temperature variations in all three sediment traps are minimal as recorded by the LDI. Accordingly, we chose to apply the Diol Index according to Rampen et al. (2008).

Potential fluvial input of organic carbon was determined by the fractional abundance of the C_{32} 1,15-diol (de Bar et al., 2016; Lattaud et al., 2017a):

$$F\text{C}_{32}\ 1,15\text{-diol} = \frac{[C_{32}\ 1,15-diol]}{[C_{28}\ 1,13-diol] + [C_{30}\ 1,13-diol] + [C_{30}\ 1,15-diol] + [C_{32}\ 1,15-diol]} \quad [9]$$

349 The fractional abundance of the C_{32} 1,15-diol was always lower than 0.23, suggesting low input of river

350 derived organic carbon (Lattaud et al., 2017a).

351

352 **3. Results**

353 **3.1 Tropical North Atlantic**

354 We have analyzed sediment trap samples from a longitudinal transect ($\sim$ 12°N) in the tropical North

355 Atlantic (two upper traps at ca. 1200 m water depth, and three lower traps at ca. 3500 m; Fig. 1), covering

356 November 2012–November 2013, as well as seven underlying surface sediments, for LCDs, LCAs and

357 GDGTs. Below we present the results for these lipid biomarkers and associated proxies.

358 **3.1.1 LCDs**

359 The LCDs detected in the sediment trap samples and surface sediments from the tropical North Atlantic

360 (Fig. 2) are the C_{28}, C_{30} and $C_{30:1}$ 1,14-, C_{28} and C_{30} 1,13-, the C_{30} 1,15-, and C_{32} 1,15-diols. We detected

361 the C_{28} 1,14- diol and C_{29}-OH fatty acid in the traps from M1 and M4, in a few samples of the M2 traps

362 and in all surface sediments. For most samples from M2U and M2L, the C_{28} 1,14-diol was often part of

363 a high background signal, making identification and quantification problematic. In these cases, 1,14-

364 diol fluxes and Diol Index were solely based on the (saturated and mono-unsaturated) C_{30} 1,14-diol.

365 The average [1,13+1,15]-diol flux is 2.6 ($\pm$ 1.0) µg m^{-2} d^{-1} at M1U, 1.4 ($\pm$ 1.2) and 1. 2 ($\pm$ 1.1) µg m^{-2} d^{-}

366 ^{1} for M2U and M2L, respectively, and 7.0 ($\pm$ 7.8) and 2.2 ($\pm$ 3.3) µg m^{-2} d^{-1} for M4U and M4L,

367 respectively (Fig. 3). The [1,13+1,15]-diol and 1,14-diol concentrations in the underlying sediments

368 vary between 0.05 µg g^{-1} and 0.50 µg g^{-1}, and between 3 ng g^{-1} and 0.06 µg g^{-1}, respectively. The 1,14-

369 diol flux for M1U averages 0.5 ($\pm$ 0.8) µg m^{-2} d^{-1} with a pronounced maximum of 3.5 µg m^{-2} d^{-1} in late

370 April (Fig. 5a), irrespective of the total mass flux. The average 1,14-diol flux at M2 is much lower and

371 similar for the upper and lower traps, being around 0.01–0.02 ($\pm$ 0.01) µg m^{-2} d^{-1}. At M4, the average

372 1,14-diol fluxes are 0.3 ($\pm$ 0.5) and 0.1 ($\pm$ 0.2) µg m^{-2} d^{-1} for the upper and lower trap, respectively.

373 There are two evident maxima in the [1,13+1,15]-diols and 1,14-diol fluxes in late April and during

374 October/November, concomitant with maxima in the total mass flux (Fig. 3d and 3e). However, in the

375   lower trap this flux maximum is distributed over two successive trap cups, corresponding to late

376   April/early May (Fig. 3e and 3j).

377   The LDI ranged between 0.95 and 0.99 in all traps, corresponding to temperatures of 26.0 to 27.3 °C

378   with no particular trends (Fig. 4). For most M2 and M4 samples the C_{28} 1,13-diol was below

379   quantification limit and, hence, LDI was always around unity, corresponding to 26.9 to 27.3 °C (Fig. 4),

380   whereas in others samples the C_{28} 1,13-diol co-eluted with cholest-5-en-7-one-3β-ol, prohibiting the

381   calculation of the LDI and Diol Index (Fig. 4 and 5). The flux-weighted annual average LDI-derived

382   SSTs are 26.6 °C for M1U, and 27.1 °C for M2U, M2L, M4U and M4L. The underlying sediment is

383   very similar, with LDI values between of 0.95 and 0.98 corresponding to 26.0 and 26.9 °C (Fig. 6). The

384   Diol Index varied from 0.03 to 0.30 in M1U, showing a pronounced maximum during spring (Fig. 5a).

385   The Diol Index at M2 ranges between 0.01 and 0.05 without an evident pattern, while the Diol Index at

386   M4 ranges from 0.01 to 0.10 and shows the same pattern in the lower and upper trap, with highest values

387   during spring (ca. 0.1), followed by a gradual decrease during summer (Fig. 5d; 5e).

388

389   **3.1.2 LCAs**

390   We detected C_{37}, C_{38} and C_{39} long-chain alkenones in the sediment trap and surface sediments. The $C_{37:3}$

391   alkenone was generally around the limit of quantification for the M2L and M4L traps, and below the

392   limit of quantification for 4 out of the 7 surface sediment samples, while the $C_{37:2}$ alkenone was always

393   sufficiently abundant. The annual mean fluxes of the C_{37} LCAs are 4.3 (± 3.5) µg m^{-2} d^{-1} for M1U, 1.2

394   (± 0.9) µg m^{-2} d^{-1} and 0.4 (± 0.2) µg m^{-2} d^{-1} for M2U and M2L, respectively, and 2.8 (± 5.0) µg m^{-2} d^{-1}

395   and 1.2 (± 2.0) µg m^{-2} d^{-1} for M4U and M4L, respectively. The concentrations of the C_{37} LCAs in the

396   underlying surface sediments range between 0.02 and 0.41 µg g^{-1}. At M4, the two total mass flux peaks

397   at the end of April and during October/November are also clearly pronounced in the C_{37} alkenone fluxes

398   (Fig. 3d, 3e and 5g), as well as the increased signal in the cup reflecting the beginning of May, which

399   follows the cup which recorded the peak in total mass flux at the end of April. The $U^{K'}_{37}$ varied from

400   0.87 to 0.93, corresponding to 25.1 to 27.0 °C (Fig. 6c) for 3 out of 7 surface sediments in which the

401    $C_{37:3}$ was above quantification limit. The flux-weighted average SSTs are 26.1 °C for M1U, 25.7 and

402   26.4 °C for M2U and M2L, respectively, and 28.2 and 27.5 °C for M4U and M4L, respectively (Fig. 6).

403   SST variations per sediment trap are generally within a 2–3 °C range (Fig. 4) with no apparent trends.

404

3.1.3 GDGTs

406   The main GDGTs detected were the isoprenoidal GDGT-0, -1, -2, -3, crenarchaeol and the isomer of

407   crenarchaeol. Branched GDGTs were typically around or below quantification limit. The average

408   iGDGT flux in M1U is 15.5 ($\pm$ 4.6) µg m^{-2} d^{-1}, 2.4 ($\pm$ 1.1) and 2.6 ($\pm$ 0.3) µg m^{-2} d^{-1} in M2U and M2L,

409   respectively, and 4.3 ($\pm$ 1.5) and 2.9 ($\pm$ 1.2) µg m^{-2} d^{-1} in M4U and M4L, respectively (Fig. 3f). The

410   surface sediments exhibit iGDGT concentrations between 0.4 and 1.7 µg g^{-1}. Sediment TEX$^H_{86}$ values

411   vary between 0.62 and 0.69, corresponding to 24.3 to 27.4 °C. The TEX$^H_{86}$ flux-weighted average SSTs

412   are 25.2 °C for M1U, 27.3 and 26.6 °C for M2U and M2L, respectively, and 27.8 and 26.7 °C for M4U

413   and M4L, respectively. SSTs vary typically within a range of 1 and 2 °C. At M2U, the TEX$^H_{86}$

414   temperatures decrease slightly (ca. 1–2 °C) between January and July (Fig. 4b).

415

3.2 Mozambique Channel

417   For two time series (November 2003–September 2007 and February 2008–February 2009), we have

418   analyzed LCDs collected in the sediment trap at 2250 m water depth as well as nearby underlying surface

419   sediments (Fig. 1). The main LCDs observed in the sediment traps and surface sediments are the C_{28}

420   1,12-, 1,13- and 1,14-diols, the C_{30} 1,13-, 1,14- and 1,15-diols and the C_{32} 1,15-diol. We also observed

421   the $C_{30:1}$ 1 1,14 diol in some trap samples, and the C_{29} 12-OH fatty acid in all trap and sediment samples.

422   In 24 samples, the C_{28} 1,13-diol co-eluted with cholest-5-en-7-one-3β-ol, and henceforth we did not

423   calculate the LDI for these samples. The C_{28} 1,14-diol was not affected by this cholest-5-en-7-one-3β-

424   ol due to its much higher abundance compared to the C_{28} 1,13-diol and the Diol Index was therefore still

425   calculated. The LDI varied between 0.94 and 0.99, i.e., close to unity, corresponding to 25.5 to 27.2 °C,

426   without an evident trend (Fig. 7a). The Diol Index ranges between 0.11 and 0.69, showing substantial

427 variation, although not with an evident trend (Fig. 7b). The average LDI-derived temperature of two

428 underlying surface sediments is 26.0 °C.

429

430 **3.3 Cariaco Basin**

431 We analyzed LCDs for two time series (May 1999–May 2000 and July 2002–July 2003) from the upper

432 (Trap A; 275 m) and the lower trap (Trap B; 455 m) in the Cariaco Basin. The main LCDs detected for

433 both time series are the C_{28} 1,14-, C_{30} 1,14-, $C_{30:1}$ 1,14-, C_{28} 1,13-, C_{30} 1,15- and C_{32} 1,15-diols, as well

434 as the C_{29} 12-OH fatty acid. For some samples we did not compute the LDI, as the C_{28} 1,13-diol co-

435 eluted with cholest-5-en-7-one-3β-ol. Similarly as for the Mozambique Channel, the C_{28} 1,14-diol was

436 not affected by this co-elution due to its much higher abundance compared to the C_{28} 1,13-diol and the

437 Diol Index was therefore still calculated. The calculated LDI values range between 24.3 and 25.3 °C

438 and 22.0 and 27.2 °C for Trap A and B of the 1999-2000 time series, respectively, with the lowest

439 temperature during winter, and the highest during summer. For the 2002-2003 time series, LDI

440 temperatures for Trap A range between 23.3 and 26.2 °C, and for Trap B between 22.5 °C and 26.5 °C.

441 For the May 1999–May 2000 time series, the Diol Index varies between 0.05 and 0.97 for Trap A, and

442 between 0.05 and 0.91 for Trap B (Fig. 8) with similar trends, i.e. the lowest values of around 0.1-0.2

443 just before the upwelling period during November, rapidly increasing towards values between ca. 0.8

444 and 1 during the upwelling season (January and February). For the time series of July 2002–July 2003,

445 the Diol Index shows similar trends, i.e. Diol Index values around 0.8-0.9 during July, which rapidly

446 decrease towards summer values of around 0.2-0.3. Similar to the 1999-2000 time series, the lowest

447 index values (ca. 0.2) are observed just before the upwelling period (during September), after which

448 they increase towards values of around 0.8-0.9 between December and March at the start of the

449 upwelling season. At the end of the upwelling season the Diol Index increases, followed by another

450 maximum of around 0.6 during May.

4. Discussion

4.1 LCD sources and seasonality

The 1,14 diols can potentially be derived from two sources, i.e. *Proboscia* diatoms (Sinninghe Damsté et al., 2003; Rampen et al., 2007) or the dictyochophyte *Apedinella radians* (Rampen et al., 2011). The non-detection of the C_{32} 1,14-diol, which is a biomarker for *Apedinella radians* (Rampen et al., 2011), and the detection of the $C_{30:1}$ 1,14 diol and C_{29} 12-OH fatty acid, which are characteristic of *Proboscia* diatoms (Sinninghe Damsté et al., 2003), suggests that *Proboscia* diatoms are most likely the source of 1,14-diols in the tropical North Atlantic, the Mozambique Channel and the Cariaco Basin.

In the Cariaco Basin, the Diol Index shows a strong correlation (visually as correlation analysis was not possible due to differently spaced data in time) with primary production rates, suggesting that *Proboscia* productivity was synchronous with total productivity (Fig. 8), although for the 1999-2000 time series there is a disagreement during January/February. Primary productivity in the Cariaco Basin is largely related to seasonal upwelling which occurs between November and May when the ITCZ is at its southern position. Hence, the Diol Index seems to be an excellent indicator of upwelling intensity in the Cariaco Basin.

The index also shows considerable variation over time in the Mozambique Channel (Fig. 7b). Previous studies have shown that upwelling occurs in the Mozambique Channel between ca. 15 and 18°S (Nehring et al., 1987; Malauene et al., 2014), i.e. at the location of our sediment trap. Upwelling is reflected by cool water events and slightly enhanced Chlorophyll *a* levels, and Malauene et al. (2014) observed cool water events at ca. two month intervals although periods of 8 to 30 days were also observed. The two main potential forcing mechanisms for upwelling in the Mozambique Channel are the East African monsoon winds and the meso-scale eddies migrating through the channel. Fallet et al. (2011) showed that subsurface temperature, current velocity and the depth of surface-mixed layer all revealed a dominant periodicity of four to six cycles per year, which is the same frequency as that of the southward migration of meso-scale eddies in the channel (Harlander et al., 2009; Ridderinkhof et al., 2010), implying that eddy passage strongly influences the water mass properties. Wavelet analysis of the Diol Index for the period 2003–2007 (supplemental Fig. S1) revealed short periods, occurring around

478   January of 2004, 2005, and 2006, of significant (above the 95 % confidence level) variability at about

479   bimonthly frequencies (60-day period). Both the frequency (bimonthly) and the timing (boreal winter)

480   of the observed time periods of enhanced Diol Index variability are similar to those of the cool water

481   events as observed by Malauene et al. (2014), associated with upwelling (Fig. 7b). The strongest

482   variability of the Diol Index at about bimonthly frequencies occurred in the first half of 2006. During

483   the same period, salinity time series showed the passage of several eddies that had a particularly strong

484   effect on the upper layer hydrography (Ullgren et al., 2012). Malauene et al. (2014) showed that neither

485   upwelling-favorable winds, nor passing eddies, can by themselves explain the observed upwelling along

486   the northern Mozambique coast. The two processes may act together, and both strongly influence the

487   upper water layer and the organisms living there, potentially including the LCD producers.

488   The least (seasonal) variation in the Diol Index is observed at M2 in the tropical North Atlantic (Fig. 5b

489   and 5c), which is likely due to its central open ocean position, associated with relatively stable,

490   oligotrophic conditions (Guerreiro et al., 2017). In contrast, M4 and M1 are closer to the south American

491   and west African coast, respectively, and thus are potentially under the influence of Amazon river runoff

492   and upwelling, respectively, and specific wind and ocean circulation regimes (see Sect. 2.1.1). However,

493   at M4, the Diol Index is also low (max. 0.1), suggesting low *Proboscia* productivity (Fig. 5d and 5e).

494   At M1, by contrast, we observe enhanced values for the Diol Index of up to ~0.3 during spring (Fig. 5a).

495   Most likely, an upwelling signal at this location is associated with the seasonal upwelling of the Guinea

496   Dome. This upwelling is generally most intense between July and October (Siedler et al., 1992), due to

497   the northward movement of the ITCZ and the resulting intensified Ekman upwelling. Specifically,

498   during this period, the trade winds are weaker, atmospheric pressure is lower, and the regional wind

499   stress is favorable to upwelling of the North Equatorial Undercurrent (Voituriez, 1981). Indeed, a

500   decrease in wind speed and increased precipitation during summer to autumn was observed (Fig. 5a)

501   which confirms that during these seasons the ITCZ was indeed at a northern position, and that during

502   2013 the upwelling associated with the Guinea Dome was most favored between July and October. The

503   timing of the Diol Index peak, i.e., between March and June is consistent with previous sediment trap

504   studies elsewhere which have shown that *Proboscia* diatoms and 1,14-diols are typically found during

505 pre-upwelling or early upwelling periods (Koning et al., 2001; Smith, 2001; Sinninghe Damsté et al.,

506 2003; Rampen et al., 2007). The surface sediment at 22° W just east of M1 also reveals the highest Diol

507 Index (0.53), likely due to its closer vicinity to the Guinea Dome center. Several studies have reported

508 *P. alata* diatoms offshore North West Africa (Lange et al., 1998; Treppke et al., 1995; Crosta et al.,

509 2012; Romero et al., 1999), pointing to *P. alata* as a plausible source organism. The sedimentary annual

510 diol indices compare well with the sediment trap indices (Fig. 6e), which is consistent with the results

511 of Rampen et al. (2008). Our results clearly show that the Diol Index reflects different things in different

512 regions. This is due to the ecology of *Proboscia* spp. where blooms occur during stratification to early

513 upwelling to postbloom, and from high nutrients to low nutrients (see Rampen et al., 2014; references

514 in Table 1). Therefore, the type of conditions reflected by the Diol Index is specific for every region.

515 To assess variations in seasonal production of 1,13- and 1,15-diols in the tropical Atlantic, for which we

516 have the most complete dataset, we calculated the flux-weighted 1,13- and 1,15-diol concentrations for

517 the different traps, and summed these per season (Fig. 9). Highest production is observed in autumn,

518 followed by summer and spring, with the lowest production during winter (~60 % compared to autumn).

519 This is in agreement with Rampen et al. (2012) who observed, for an extensive set of surface sediments,

520 the strongest correlation between LDI and SST for autumn, suggesting that production of the source

521 organisms of the LDI mainly occurs during autumn. At M4, there are two evident peaks in the 1,13- and

522 1,15-diol fluxes at the end of April and October 2013. These maxima correlate with peaks in other lipid

523 biomarker fluxes (i.e., 1,14-diols, C_{37} alkenones and iGDGTs), total mass flux, calcium carbonate

524 ($CaCO_3$), OM and the residual mass flux which includes the deposition flux of Saharan dust (Korte et

525 al., 2017). According to Guerreiro et al. (2017), the maximum in total mass flux at the end of April 2013

526 is likely caused by enhanced export production due to nutrient enrichment as a result of wind-forced

527 vertical mixing. The peak at the end of October 2013, is likely associated with discharge from the

528 Amazon River. Moreover, both peaks are concomitant with prominent dust flux maxima, suggesting

529 that Saharan dust also acted as nutrient fertilizer (Korte et al., 2017; Guerreiro et al., 2017). Guirreirro

530 et al. (2017) suggested that during the October-November event the Amazon River may not only have

531 acted as nutrient supplier, but also as buoyant surface density retainer of dust-derived nutrients in the

532 surface waters, resulting in the development of algal blooms within just a few days, potentially

533 explaining the peak 1,13- and 1,15-diol fluxes, as well as the peak fluxes of the other lipid biomarkers.

534 However, they might also partially result from enhanced particle settling, caused by e.g. dust ballasting

535 or faecal pellets of zooplankton (see Guerreiro et al. 2017 and references therein). This agrees with the

536 results of Schreuder et al. (2018a) who show that the *n*-alkane flux also peaks concomitant with the

537 peaks in total mass flux and biomarkers, whereas *n*-alkanes are terrestrial derived (predominantly

538 transported by dust) and increased deposition can therefore not result from increased primary

539 productivity in the surface waters.

540 The C_{37} alkenone flux at M4U also reveals these two distinct maxima at the end of April and October

541 during 2013 (Fig. 5g). Interestingly, this flux, as well as the alkenone flux at M2U, is consistent with

542 coccolith export fluxes of the species *Emiliania huxleyi* and *Gephyrocapsa oceanica* (Guerreiro et al.,

543 2017). In fact, when we combine the coccolith fluxes of both species, we observe strong correlations

544 with the C_{37} alkenone fluxes for both M2U and M4U (Fig. 5f and 5g, respectively; $r = 0.77$ and 0.92 for

545 M2U and M4U, respectively; p-values < 0.001). This implies that these two species are the main LCA

546 producers in the tropical North Atlantic, which agrees with previous findings (e.g., Marlowe et al., 1984;

547 Brassell, 2014; Conte et al., 1994; Volkman et al., 1995).

548

4.2 Preservation of LCDs

550 The sediment trap data from the North Atlantic can be used to assess the relative preservation of LCDs,

551 as well as other proxy lipid biomarkers, by comparing the flux-weighted concentration in the traps with

552 the concentrations in the surface sediments. For all four biomarker groups, i.e., C_{37} alkenones, iGDGTs,

553 1,14-diols and 1,13- and 1,15-diols, we observe that in general the flux-weighted concentrations are

554 higher in the upper traps (ca. 1200 m) as compared to the lower traps (ca. 3500 m; Fig. 2) by a factor of

555 between 1.2 and 4.4, implying degradation during settling down the water column. The concentrations

556 in the surface sediments are 2 to 3 orders of magnitude lower in concentration (i.e., between 0.1–1.5 %

557 of upper trap signal), implying that degradation of lipids is mainly taking place at the water-sediment

558 surface rather than the water column. A similar observation was made for levoglucosan in these sediment

559 traps (Schreuder et al., 2018b). Both are functionalized polar lipids with alcohol groups and thus are

560 chemically relatively similar when compared to e.g. fatty acids (carboxyl group) or *n*-alkanes (no

561 functional groups). These degradation rates are likely linked to the extent of the oxygen exposure time

562 (Hartnett et al., 1998; Hedges et al., 1999) at the seafloor (Hartnett et al., 1998; Sinninghe Damsté et al.,

563 2002), since during settling the lipids are exposed to oxygen for weeks, whereas for surface sediments

564 this is typically decades to centuries. Our results compare well with several other sediment trap studies

565 which showed that LCDs, LCAs and iGDGTs generally have a preservation factor of around 1 %

566 (surface sediment vs. trap) (e.g., Prahl et al., 2000; Wakeham et al., 2002; Rampen et al., 2007;

567 Yamamoto et al., 2012).

568 We have also identified the C_{30} and C_{32} 1,15-keto-ol in the Atlantic as well as the Mozambique and

569 Cariaco sediment traps and surface sediments. These lipids are structurally related to LCDs and occur

570 ubiquitously in marine sediments (e.g., Versteegh et al., 1997; 2000; Bogus et al., 2012; Rampen et al.,

571 2007; Sinninghe Damsté et al., 2003; Wakeham et al., 2002; Jiang et al., 1994), and were inferred to be

572 oxidation products of LCDs (Ferreira et al., 2001; Bogus et al., 2012; Sinninghe Damsté et al., 2003).

573 We have not detected 1,14-keto-ols, which supports the hypothesis of Ferreira et al. (2001) and

574 Sinninghe Damsté et al. (2003) that the silica frustules of *Proboscia* diatoms sink relatively fast and thus

575 are exposed to oxygen for a shorter period than the producers of 1,13- and 1,15-diols, and thus less

576 affected by oxidation. Alternatively, the keto-ols are not oxidation products but are produced by

577 unknown organisms in the water column. In fact, Méjanelle et al. (2003) observed trace amounts of C_{30}

578 1,13- and C_{32} 1,15-keto-ols in cultures of the marine eustigmatophyte *Nannochloropsis gaditana*. Thus,

579 an alternative explanation for the non-detection of 1,14-keto-ols is that, in contrast to the 1,15-keto-ols,

580 they were not produced in the water column.

581 For both the tropical Atlantic and the Cariaco Basin, we observe highly similar LDI values for the upper

582 and the lower traps. In the Atlantic there is no statistical difference between upper and lower trap that

583 are 2200 m apart (two-tailed $p > 0.8$), but we have too little data for the Cariaco Basin for statistical

584 comparison (Fig. 6b, 8c and 8f). This suggests that degradation in the water column does not affect the

585 LDI proxy. This is in agreement with the study of Reiche et al. (2018) who performed a short-term

586   degradation experiment (< 1 year) and found that the LDI index was not affected by oxic exposure on

587   short time scales. However, the oxygen exposure time on the seafloor is much longer, and Rodrigo-

588   Gámiz et al. (2016) showed for sediments in the Arabian Sea, deposited under a range of bottom water

589   oxygen conditions, that different LCDs had different degradation rates, which compromised the LDI

590   ratio. For the three sites in the tropical North Atlantic, we have calculated the flux-weighted average

591   proxy values for every sediment trap and compare these with the underlying surface sediments (Fig. 6b-

592   6e). For all indices, i.e., Diol Index, LDI, $U^{K'}_{37}$ and TEX_{86}, we observe very good correspondence

593   between the sediment trap and surface sediment values, implying minimal alteration of the proxies after

594   settling and during burial. Similarly, for the Mozambique Channel, the mean Diol Index and LDI from

595   the sediment trap (i.e., 0.41 and 0.97, respectively) are very similar to the surface sediment values (i.e.,

596   0.42 and 0.95, respectively). In agreement with the consistent diol indices, we observe that all individual

597   LCDs are also preserved relatively equally in the tropical Atlantic (1.2-4.3 % at station M1, 0.1-2.9 %

598   at station M2 and 0.03-0.16 % at station M4). This contrasts with the findings of Rodrigo-Gámiz et al.

599   (2016) who found that the 1,15-diols have the highest degradation rate, followed by the 1,14- and 1,13-

600   diols. Only the C_{32} 1,15-diol seems relatively better preserved than the other LCDs at all three North

601   Atlantic mooring sites (Fig. 2), suggesting that the C_{32} 1,15-diol is less impacted by degradation. The

602   C_{32} 1,15-diol likely partially derives from the same source as the other 1,13- and 1,15-diols, but is also

603   produced in fresh water systems (e.g., Versteegh et al., 1997; 2000; Rampen et al., 2014b; de Bar et al.,

604   2016; Lattaud et al., 2017a; 2017b). Hence, the different preservation characteristics might be the result

605   of a different source for this LCD.

606

607   **4.3 Relationship between LDI and SST**

608   In the tropical Atlantic and Mozambique Channel, the LDI-derived SSTs show minimal variability (<2

609   °C), while in the Cariaco Basin we observe much larger changes that range from 22.0 °C to 27.2 °C

610   (Fig. 8). Both time series in the Cariaco Basin show low temperatures between November and May

611   associated with the seasonal upwelling and surface water cooling, and significantly higher temperatures

612   during the rainy summer. However, during the warmest periods, the LDI temperatures are generally

613   lower than measured at the surface by CTD, whereas during the colder phases, the LDI agrees well with

614   the measurements. The LDI calibration reaches unity at 27.4 °C, and therefore it is not possible to resolve

615   the highest temperatures which are between ca. 28 and 30 °C. However, the LDI-derived temperatures

616   are sometimes well below 27.4 °C where the CTD data suggest SSTs > 28 °C. Consequently, the LDI-

617   based temperatures agree with CTD-based SSTs within calibration error for most of the record, but

618   during summer when SST is highest, are offset outside the calibration error (ΔT ~2.5-4.5 °C).

619   Interestingly, the $U^{K'}_{37}$- and TEX^H_{86}-derived temperature trends show the same phenomenon (Turich et

620   al., 2013; Fig. 8), where the proxy temperatures are cooler than the measured temperatures during the

621   warmer months. However, in contrast to the $U^{K'}_{37}$ and LDI, the TEX^H_{86} also overestimates SST during

622   the cold months. For $U^{K'}_{37}$, Turich et al. (2013) pointed out that a time lag between synthesis, export and

623   deposition could potentially explain the difference between the proxy and CTD temperatures. However,

624   previous analysis of plankton biomass, primary productivity, bio-optical properties and particulate

625   organic carbon fluxes for the same time period (Müller-Karger et al., 2004), as well as the total mass

626   and terrigenous fluxes assessed by Turich et al. (2013) showed best correlation at zero-time lag on the

627   basis of their 14-day sample interval. We compared our LDI temperature estimates with monthly CTD

628   measurements between 0 and 50 m depth, the temperature at depth of maximum primary productivity

629   and the temperature at the chlorophyll maximum (Turich et al., 2013; http://www.imars.usf.edu/cariaco)

630   (Fig. 10). During the upwelling season, temperatures are significantly lower due to the upward migration

631   of isotherms, whereas during the non-upwelling period, temperatures are higher, particularly in the upper

632   20 m, and the water column is more stratified (Fig. 10). LDI underestimates SST during stratification,

633   which suggests that the LCD producers may thrive at depths of ca. 20–30 m. During upwelling, LDI-

634   temperatures agree better with SST, implying that the habitat of the LCD producers potentially was

635   closer to the surface, coincident with the shoaling of the nutricline and thermocline (Fig. 10). However,

636   these absolute differences in LDI-temperatures are generally within the calibration error (2 °C), and

637   these seasonal variations in LDI-temperatures should thus be interpreted with caution. Turich et al.

638   (2003) found that the $U^{K'}_{37}$-derived temperatures agreed reasonably well with the measured temperatures

639   at the chlorophyll maximum, which is generally found below 20 m depth (average 30–34 m depth;

640   ranging between 1 and 55 m) in the Cariaco Basin. The LDI temperatures are almost always higher than

641   the temperatures at the chlorophyll maximum (Fig. 10), and higher than the temperatures at 30 m depth,

642   implying that the LDI producers may reside in the upper 30 m of the water column, which is consistent

643   with the results of Rampen et al. (2012), who showed that LDI-derived temperatures have the strongest

644   correlation with temperatures of the upper 20 m of the water column. This also agrees with Balzano et

645   al. (2018) who observed highest LCD abundances within the upper 20 m of the water column in the

646   Tropical Atlantic.

647   In the Mozambique Channel, the LDI temperature variations are much smaller (< 2 °C; Fig. 7a) than the

648   seasonal SST variation ranging between ca. 24.5 and 30.5 °C. Accordingly, during the warmest months

649   of the year, the difference between LDI-derived and satellite-derived SST is outside of the calibration

650   error (i.e., > 2 °C). However, this is similar to the $U^{K'}_{37}$ and TEX^{H}_{86} which also did not reveal seasonal

651   variations. This lack of seasonality was explained by lateral advection and re-suspension of fine

652   sediment material by migrating meso-scale eddies and thus ending up in the deeply moored sediment

653   trap (Fallet et al., 2011; 2012). Most likely, this also explains the lack of seasonal variation in our LDI

654   record (Fig. 7a). Nevertheless, the average LDI temperature for the sediment trap of 26.4 °C agrees

655   reasonably well with the annual mean satellite-derived SST of 27.6 °C for the sampled years.

656   Additionally, there is a good agreement with the average LDI temperature of 26.0 °C for two underlying

657   surface sediments, as well as with the decadal average SST of 26.7 °C for 1955-2012 (Locarnini et al.,

658   2013) given by the World Ocean Atlas (2013). For the North Atlantic, we also observe rather constant

659   LDI temperatures during the year (Fig. 4) which contrasts with seasonal variations in satellite SSTs of

660   ca. 3 to 5 °C. Nevertheless, differences are mostly within the calibration error, except at M1 and M2

661   where during winter and spring LDI-derived temperatures are between 0.5 and 2.8 °C higher than

662   satellite SSTs. Similar to the LDI, also the TEX^{H}_{86} and $U^{K'}_{37}$-derived SSTs for the tropical Atlantic

663   sediment traps do not reveal clear seasonal variation. As all three proxies show minimal seasonal

664   variability, this might indicate that the lipids are potentially allochtonous and partially derive from

665   distant regions, resulting in an integrated average temperature signal, similar to the Mozambique

666   Channel. Nevertheless, the flux-weighted annual LDI temperatures of the tropical Atlantic sediment

667   traps (26.6 for M1 and 27.1 °C for M2 and M4) agree well with the annual mean satellite-derived SSTs

668   of 26.1, 26.0 and 27.5 °C for M1, M2 and M4, respectively. Moreover, the LDI-derived temperatures in

669   the underlying sediments (26.5, 26.6 and 26.7 °C, respectively) do not only agree well with those found

670   in a single year in the sediment traps but also with the decadal average SSTs for 1955 to 2012 (26.2,

671   27.1 and 26.3 °C, respectively; Locarnini et al., 2013; Fig. 6b).

672

673   **5. Conclusions**

674   In this study we have evaluated LCD-based proxies, particularly the LDI, in sediment trap time series

675   from five sites in the tropical North Atlantic, the Cariaco Basin and the Mozambique Channel. For the

676   North Atlantic we found that in the water column ca. 25–85 % of the export of these lipid biomarkers is

677   preserved during settling from 1200m to 3500m, and that generally less than 2 % was preserved in the

678   surface sediments. Despite substantial degradation at the seafloor, likely linked to the prolonged oxygen

679   exposure time, LCD-derived temperatures from the sediments are generally very similar to the annual

680   mean LCD-derived temperatures in both the deep and shallow traps as well as to annual mean SST for

681   the specific sampling year and on decadal time scales for the specific sites. In the Cariaco Basin we

682   observe a seasonal signal in the LDI linked to the upwelling season reflecting temperatures of the upper

683   ca. 30 m of the water column. The LDI temperatures in the Mozambique Channel and the tropical

684   Atlantic reveal minimal seasonal change although seasonal SST contrasts amount to 3-5°C. For the

685   Mozambique Channel this is likely caused by lateral advection of re-suspended sediment by meso-scale

686   eddy migration, a signal not substantially altered by diagenesis. Seasonal variations in the Diol Index

687   are minimal in the central and western North Atlantic and 1,14-diol concentrations are rather low,

688   implying little *Proboscia* diatom productivity. However, in the eastern Atlantic closest to the African

689   continent, the Diol Index attains a clear spring maximum that is likely associated with upwelling in the

690   Guinea Dome during summer to autumn, suggesting the Diol Index reflects a pre-upwelling signal,

691   consistent with the current knowledge on *Proboscia* ecology. In the Cariaco Basin, controlled by

692   seasonal upwelling, the Diol Index reveals the same clear seasonal trend observed in primary

693   productivity, arguing that for this location the Diol Index is an excellent indicator of upwelling intensity.

694

695 **Data availability**. The data reported in this paper is archived in PANGAEA (www.pangaea.de.)

696

697 **Author contributions**. MWdB, JSSD, and SS designed the experiments and MWdB carried them out.

698 JU carried out the time-series analysis. JBWS, GJAB, and RCT deployed sediment traps and collected

699 sediment trap materials. MWdB prepared the paper with contributions from all coauthors.

700

701 **Competing interests**. The authors declare that they have no conflict of interest.

702

703 **Acknowledgements.** We are grateful to Laura Schreuder and Denise Dorhout for analytical support,

704 Wim Boer for help with MatLab calculations (BAYSPLINE), Laura Korte and Catarina Guerreiro for

705 constructive discussions, and Isla Castañeda, Ulrike Fallet and Courtney Turich for providing and

706 working up samples. This research has been funded by the European Research Council (ERC) under the

707 European Union's Seventh Framework Program (FP7/2007-2013) ERC grant agreement [339206] to

708 S.S. and ERC grant agreement [311152] as well as NWO project [822.01.008] to J-B.S.. S.S. and

709 J.S.S.D. receive financial support from the Netherlands Earth System Science Centre (NESSC) through

710 a gravitation grant from the Dutch ministry for Education, Culture and Science (grant number

711 024.002.001).

712

713 **References**

714   Araujo, M., Noriega, C., Hounsou-gbo, G. A., Veleda, D., Araujo, J., Bruto, L., Feitosa, F.,

715 Flores-Montes, M., Lefevre, N., Melo, P., Otsuka, A., Travassos, K., Schwamborn, R., and Neumann-

716 Leitao, S.: A Synoptic Assessment of the Amazon River-Ocean Continuum during Boreal Autumn:

717 From Physics to Plankton Communities and Carbon Flux, Front. Microbiol., 8,

718 https://doi.org/10.3389/fmicb.2017.01358, 2017.

719   Balzano, S., Lattaud, J., Villanueva, L., Rampen, S. W., Brussaard, C. P. D., van Bleijswijk, J.,
720   Bale, N., Sinninghe Damsté, J. S., and Schouten, S.: A quest for the biological sources of long chain
721   alkyl diols in the western tropical North Atlantic Ocean, Biogeosciences, 15, 5951-5968,
722   https://doi.org/10.5194/bg-15-5951-2018, 2018.

723   Biastoch, A., and Krauss, W.: The Role of Mesoscale Eddies in the Source Regions of the
724   Agulhas Current, J. Phys. Oceanogr., 29, 2303-2317, https://doi.org/10.1175/1520-
725   0485(1999)029<2303:Tromei>2.0.Co;2, 1999.

726   Bogus, K. A., Zonneveld, K. A. F., Fischer, D., Kasten, S., Bohrmann, G., and Versteegh, G. J.
727   M.: The effect of meter-scale lateral oxygen gradients at the sediment-water interface on selected
728   organic matter based alteration, productivity and temperature proxies, Biogeosciences, 9, 1553-1570,
729   https://doi.org/10.5194/bg-9-1553-2012, 2012.

730   Brassell, S. C., Eglinton, G., Marlowe, I. T., Pflaumann, U., and Sarnthein, M.: Molecular
731   stratigraphy – A new tool for climatic assessment, Nature, 320, 129-133,
732   https://doi.org/10.1038/320129a0, 1986.

733   Brassell, S. C.: Climatic influences on the Paleogene evolution of alkenones, Paleoceanography,
734   29, 255-272, https://doi.org/10.1002/2013pa002576, 2014.

735   Chen, W. W., Mohtadi, M., Schefuss, E., and Mollenhauer, G.: Organic-geochemical proxies
736   of sea surface temperature in surface sediments of the tropical eastern Indian Ocean, Deep-Sea Res. Pt.
737   I, 88, 17-29, https://doi.org/10.1016/j.dsr.2014.03.005, 2014.

738   Coles, V. J., Brooks, M. T., Hopkins, J., Stukel, M. R., Yager, P. L., and Hood, R. R.: The
739   pathways and properties of the Amazon River Plume in the tropical North Atlantic Ocean, J. Geophys.
740   Res-Oceans, 118, 6894-6913, https://doi.org/10.1002/2013jc008981, 2013.

741   Conte, M. H., Thompson, A., and Eglinton, G.: Primary production of lipid biomarker
742   compounds by *Emiliania Huxleyi* – Results from an experimental mesocosm study in fjords of
743   southwestern Norway, Sarsia, 79, 319-331, https://doi.org/10.1080/00364827.1994.10413564, 1994.

744   Conte, M. H., Sicre, M. A., Ruhlemann, C., Weber, J. C., Schulte, S., Schulz-Bull, D., and
745   Blanz, T.: Global temperature calibration of the alkenone unsaturation index $U^{K'}_{37}$ in surface waters and
746   comparison with surface sediments, Geochem. Geophy. Geosy., 7,
747   https://doi.org/10.1029/2005GC001054, 2006.

748   Cropper, T. E., Hanna, E., and Bigg, G. R.: Spatial and temporal seasonal trends in coastal
749   upwelling off Northwest Africa, 1981-2012, Deep-Sea Res. Pt. I, 86, 94-111,
750   https://doi.org/10.1016/j.dsr.2014.01.007, 2014.

751   Crosta, X., Romero, O. E., Ther, O., and Schneider, R. R.: Climatically-controlled siliceous
752 productivity in the eastern Gulf of Guinea during the last 40 000 yr, Clim. Past, 8, 415-431,
753 https://doi.org/10.5194/cp-8-415-2012, 2012.

754   de Bar, M. W., Dorhout, D. J. C., Hopmans, E. C., Rampen, S. W., Sinninghe Damsté, J. S., and
755 Schouten, S.: Constraints on the application of long chain diol proxies in the Iberian Atlantic margin,
756 Org. Geochem., 101, 184-195, https://doi.org/10.1016/j.orggeochem.2016.09.005, 2016.

757   de Jonge, C., Hopmans, E. C., Zell, C. I., Kim, J. H., Schouten, S., and Sinninghe Damsté, J. S.:
758 Occurrence and abundance of 6-methyl branched glycerol dialkyl glycerol tetraethers in soils:
759 Implications for palaeoclimate reconstruction, Geochim. Cosmochim. Ac., 141, 97-112,
760 https://doi.org/10.1016/j.gca.2014.06.013, 2014.

761   de Jonge, C., Stadnitskaia, A., Hopmans, E. C., Cherkashov, G., Fedotov, A., Streletskaya, I.
762 D., Vasiliev, A. A., and Sinninghe Damsté, J. S.: Drastic changes in the distribution of branched
763 tetraether lipids in suspended matter and sediments from the Yenisei River and Kara Sea (Siberia):
764 Implications for the use of brGDGT-based proxies in coastal marine sediments, Geochim. Cosmochim.
765 Ac., 165, 200-225, https://doi.org/10.1016/j.gca.2015.05.044, 2015.

766   Doi, T., Tozuka, T., and Yamagata, T.: Interannual variability of the Guinea Dome and its
767 possible link with the Atlantic Meridional Mode, Clim. Dynam., 33, 985-998,
768 https://doi.org/10.1007/s00382-009-0574-z, 2009.

769   Duce, R. A., Liss, P. S., Merrill, J. T., Atlas, E. L Buat-Menard, P., Hicks, B. B., Miller, J. M.,
770 Prospero, J. M., Arimoto, R., Church, T. M., Ellis, W., Galloway, J. N., Hansen, L., Jickells, T. D.,
771 Knap, A. H., Reinhardt, K. H., Schneider, B., Soudine, A., Tokos, J. J., Tsunogai, S., Wollast, R., and
772 Zhou, M.: The Atmospheric Input of Trace Species to the World Ocean, Global Biogeochem. Cy., 5,
773 193-259, https://doi.org/10.1029/91gb01778, 1991.

774   Fallet, U., Brummer, G. J., Zinke, J., Vogels, S., and Ridderinkhof, H.: Contrasting seasonal
775 fluxes of planktonic foraminifera and impacts on paleothermometry in the Mozambique Channel
776 upstream of the Agulhas Current, Paleoceanography, 25, 12, https://doi.org/10.1029/2010pa001942,
777 2010.

778   Fallet, U., Ullgren, J. E., Castaneda, I. S., van Aken, H. M., Schouten, S., Ridderinkhof, H., and
779 Brummer, G. J. A.: Contrasting variability in foraminiferal and organic paleotemperature proxies in
780 sedimenting particles of the Mozambique Channel (SW Indian Ocean), Geochim. Cosmochim. Ac., 75,
781 5834-5848, https://doi.org/10.1016/j.gca.2011.08.009, 2011.

782   Fallet, U., Castaneda, I. S., Aneurin, H. E., Richter, T. O., Boer, W., Schouten, S., and Brummer,
783 G. J.: Sedimentation and burial of organic and inorganic temperature proxies in the Mozambique

784 Channel, SW Indian Ocean, Deep-Sea Res. Pt. I, 59, 37-53, https://doi.org/10.1016/j.dsr.2011.10.002,
785 2012.

786 Ferreira, A. M., Miranda, A., Caetano, M., Baas, M., Vale, C., and Sinninghe Damsté, J. S.:
787 Formation of mid-chain alkane keto-ols by post-depositional oxidation of mid-chain diols in
788 Mediterranean sapropels, Org. Geochem., 32, 271-276, https://doi.org/10.1016/S0146-6380(00)00181-
789 9, 2001.

790 Frouin, R., Franz, B. A., Werdell, P. J.: The SeaWiFS PAR product., In: S.B. Hooker and E.R.
791 Firestone, Algorithm Updates for the Fourth SeaWiFS Data Reprocessing, NASA Tech. Memo. 2003–
792 206892, Volume 22, NASA Goddard Space Flight Center, Greenbelt, Maryland, 46-50. The SeaWiFS
793 PAR product, 2003.

794 Gibbons, J. D. & Chakraborty, S.: Nonparametric Statistical Inference. Fourth Edition. Marcel
795 Dekker Inc., New York, 645 pp. ISBN: 0-8247-4052-1, 2003.

796 Goddard Earth Sciences Data and Information Services Center, TRMM (TMPA-RT) Near Real-
797 Time Precipitation L3 1 day 0.25 degree x 0.25 degree V7, Greenbelt, MD, Goddard Earth Sciences
798 Data and Information Services Center (GES DISC),
799 http://disc.gsfc.nasa.gov/datacollection/TRMM_3B42RT_Daily_7.html, 2016.

800 Goñi, M. A., Woodworth, M. P., Aceves, H. L., Thunell, R. C., Tappa, E., Black, D., Müller-
801 Karger, F., Astor, Y., and Varela, R.: Generation, transport, and preservation of the alkenone-based U^{K}_{37}
802 sea surface temperature index in the water column and sediments of the Cariaco Basin (Venezuela),
803 Global Biogeochem. Cy., 18, 1-21, https://doi.org/10.1029/2003GB002132, 2004.

804 Gordon, A. L.: Inter-ocean exchange of thermocline water, J. Geophys. Res-Oceans, 91, 5037-
805 5046, https://doi.org/10.1029/JC091iC04p05037, 1986.

806 Goudie, A. S., and Middleton, N. J.: Saharan dust storms: nature and consequences, Earth-Sci.
807 Rev., 56, 179-204, https://doi.org/10.1016/S0012-8252(01)00067-8, 2001.

808 Guerreiro, C. V., Baumann, K. H., Brummer, G. J. A., Fischer, G., Korte, L. F., Merkel, U., Sa,
809 C., de Stigter, H., and Stuut, J. B. W.: Coccolithophore fluxes in the open tropical North Atlantic:
810 influence of thermocline depth, Amazon water, and Saharan dust, Biogeosciences, 14, 4577-4599,
811 https://doi.org/10.5194/bg-14-4577-2017, 2017.

812 Guerreiro, C. V., Baumann, K.-H., Brummer, G.-J. A., Fischer, G., Korte, L. F., Sá, C. and
813 Stuut, J.-B. W.: Wind-forced transatlantic gradients in coccolithophore species fluxes, Submitted to
814 Prog. Oceanogr. (in revision), 2018.

Harlander, U., Ridderinkhof, H., Schouten, M. W., and de Ruijter, W. P. M.: Long-term observations of transport, eddies, and Rossby waves in the Mozambique Channel, J. Geophys. Res-Oceans, 114, https://doi.org/10.1029/2008jc004846, 2009.

Hartnett, H. E., Keil, R. G., Hedges, J. I., and Devol, A. H.: Influence of oxygen exposure time on organic carbon preservation in continental margin sediments, Nature, 391, https://doi.org/10.1038/35351 572-574, 1998.

Hedges, J. I., Sheng Hu, F., Devol, A. H., Hartnett, H. E., Tsamakis, E., and Keil, R. G.: Sedimentary organic matter preservation: a test for selective degradation under oxic conditions, Am. J. Sci., 299, 529-555, https://doi.org/10.2475/ajs.299.7-9.529 1999.

Herndl, G. J., Reinthaler, T., Teira, E., van Aken, H., Veth, C., Pernthaler, A., and Pernthaler, J.: Contribution of *Archaea* to total prokaryotic production in the deep Atlantic Ocean, Appl. Environ. Microb., 71, 2303-2309, https://doi.org/10.1128/aem.71.5.2303-2309.2005, 2005.

Honjo, S., and Doherty, K. W.: Large aperture time-series sediment traps; design objectives, construction and application, Deep Sea Res., 35, 133-149, https://doi.org/10.1016/0198-0149(88)90062-3, 1988.

Hopmans, E. C., Weijers, J. W. H., Schefuß, E., Herfort, L., Sinninghe Damsté, J. S., and Schouten, S.: A novel proxy for terrestrial organic matter in sediments based on branched and isoprenoid tetraether lipids, Earth Planet. Sc. Lett., 224, 107-116, https://doi.org/10.1016/j.epsl.2004.05.012, 2004.

Hopmans, E. C., Schouten, S., and Sinninghe Damsté, J. S.: The effect of improved chromatography on GDGT-based palaeoproxies, Org. Geochem., 93, 1-6, http://dx.doi.org/10.1016/j.orggeochem.2015.12.006, 2016.

Huffman, G.J., Adler, R.F., Bolvin, D.T., Gu, G., Nelkin, E.J., Bowman, K.P., Hong, Y., Stocker, E.F., Wolff, D.B.: The TRMM Multi-satellite Precipitation Analysis: Quasi- Global, Multi-Year, Combined-Sensor Precipitation Estimates at Fine Scale. J. Hydrometeor. 8 (1), 38-55, https://doi.org/10.1175/JHM560.1, 2007.

Hughen, K. A., Overpeck, J. T., Peterson, L. C., and Anderson, R. F.: The nature of varved sedimentation in the Cariaco Basin, Venezuela, and its palaeoclimatic significance, Geological Society, London, Special Publications, 116, 171-183, https://doi.org/10.1144/gsl.Sp.1996.116.01.15, 1996.

Hughen, K. A., Overpeck, J. T., Lehman, S. J., Kashgarian, M., Southon, J., Peterson, L. C., Alley, R., and Sigman, D. M.: Deglacial changes in ocean circulation from an extended radiocarbon calibration, Nature, 391, 65-68, https://doi.org/10.1038/34150, 1998.

Huguet, C., Hopmans, E. C., Febo-Ayala, W., Thompson, D. H., Sinninghe Damsté, J. S., and Schouten, S.: An improved method to determine the absolute abundance of glycerol dibiphytanyl

848   glycerol   tetraether   lipids,   Org.   Geochem.,   37,   1036-1041,
849   https://doi.org/10.1016/j.orggeochem.2006.05.0082006.

850   Huguet, C., Schimmelmann, A., Thunell, R., Lourens, L. J., Sinninghe Damsté, J. S., and
851   Schouten, S.: A study of the TEX$_{86}$ paleothermometer in the water column and sediments of the Santa
852   Barbara Basin, California, Paleoceanography, 22, https://doi.org/10.1029/2006pa001310, 2007.

853   Jiang, S., O'Leary, T., Volkman, J. K., Zhang, H., Jia, R., Yu, S., Wang, Y., Luan, Z., Sun, Z.,
854   and Jiang, R.: Origins and simulated thermal alteration of sterols and keto-alcohols in deep-sea marine-
855   sediments of the Okinawa Trough, Org. Geochem., 21, 415-422, https://doi.org/10.1016/0146-
856   6380(94)90203-8, 1994.

857   Jonas, A. S., Schwark, L., and Bauersachs, T.: Late Quaternary water temperature variations of
858   the Northwest Pacific based on the lipid paleothermometers TEX$_{86}^{H}$, U$^{K'}_{37}$ and LDI, Deep-Sea Res. Pt.
859   I, 125, 81-93, http://doi.org/10.1016/j.dsr.2017.04.018, 2017.

860   Karner, M. B., DeLong, E. F., and Karl, D. M.: Archaeal dominance in the mesopelagic zone
861   of the Pacific Ocean, Nature, 409, 507-510, https://doi.org/10.1038/35054051, 2001.

862   Kim, J.-H., Schouten, S., Hopmans, E. C., Donner, B., and Sinninghe Damsté, J. S.: Global
863   sediment core-top calibration of the TEX$_{86}$ paleothermometer in the ocean, Geochim. Cosmochim. Ac.,
864   72, 1154-1173, https://doi.org/10.1016/j.gca.2007.12.010, 2008.

865   Kim, J.-H., van der Meer, J., Schouten, S., Helmke, P., Willmott, V., Sangiorgi, F., Koc, N.,
866   Hopmans, E. C., and Sinninghe Damsté, J. S.: New indices and calibrations derived from the distribution
867   of crenarchaeal isoprenoid tetraether lipids: Implications for past sea surface temperature
868   reconstructions, Geochim. Cosmochim. Ac., 74, 4639-4654, https://doi.org/10.1016/j.gca.2010.05.027,
869   2010.

870   Kim, J.-H., Romero, O. E., Lohmann, G., Donner, B., Laepple, T., Haam, E., and Sinninghe
871   Damsté, J. S.: Pronounced subsurface cooling of North Atlantic waters off Northwest Africa during
872   Dansgaard–Oeschger   interstadials,   Earth   Planet.   Sc.   Lett.,   339-340,   95-102,
873   https://doi.org/10.1016/j.epsl.2012.05.018, 2012.

874   Kim, J.-H., Schouten, S., Rodrigo-Gámiz, M., Rampen, S., Marino, G., Huguet, C., Helmke, P.,
875   Buscail, R., Hopmans, E. C., Pross, J., Sangiorgi, F., Middelburg, J. B. M., and Sinninghe Damsté, J.
876   S.: Influence of deep-water derived isoprenoid tetraether lipids on the TEX$_{86}^{H}$ paleothermometer in the
877   Mediterranean   Sea,   Geochim.   Cosmochim.   Ac.,   150,   125-141,
878   https://doi.org/10.1016/j.gca.2014.11.017, 2015.

879   Koning, E., van Iperen, J. M., van Raaphorst, W., Helder, W., Brummer, G.-J. A., and van
880   Weering, T. C. E.: Selective preservation of upwelling-indicating diatoms in sediments off Somalia,

881   NW Indian Ocean, Deep-Sea Res. Pt. I, 48, 2473-2495, https://doi.org/10.1016/S0967-0637(01)00019-
882   X, 2001.

883   Korte, L. F., Brummer, G. J. A., van der Does, M., Guerreiro, C. V., Hennekam, R., van Hateren,
884   J. A., Jong, D., Munday, C. I., Schouten, S., and Stuut, J. B. W.: Downward particle fluxes of biogenic
885   matter and Saharan dust across the equatorial North Atlantic, Atmos. Chem. Phys., 17, 6023-6040,
886   https://doi.org/10.5194/acp-17-6023-2017, 2017.

887   Lange, C. B., Romero, O. E., Wefer, G., and Gabric, A. J.: Offshore influence of coastal
888   upwelling off Mauritania, NW Africa, as recorded by diatoms in sediment traps at 2195 m water depth,
889   Deep-Sea Res. Pt. I, 45, 986-1013, https://doi.org/10.1016/s0967-0637(97)00103-9 1998.

890   Lattaud, J., Kim, J.-H., De Jonge, C., Zell, C., Sinninghe Damsté, J. S., and Schouten, S.: The
891   C_{32} alkane-1,15-diol as a tracer for riverine input in coastal seas, Geochim. Cosmochim. Ac., 202, 146-
892   158, http://doi.org/10.1016/j.gca.2016.12.030, 2017a.

893   Lattaud, J., Dorhout, D., Schulz, H., Castañeda, I. S., Schefuß, E., Sinninghe Damsté, J. S., and
894   Schouten, S.: The C_{32} alkane-1,15-diol as a proxy of late Quaternary riverine input in coastal margins,
895   Clim. Past, 13, 1049-1061, http://doi.org/10.5194/cp-13-1049-2017, 2017b.

896   Lee, T., Lagerloef, G., Gierach, M.M., Kao, H.-Y., Yueh, S., Dohan, K.: Aquarius reveals
897   salinity   structure   of   tropical   instability   waves,   Geophys.   Res.   Lett.,   39,   L12610,
898   https://doi.org/10.1029/2012GL052232, 2012.

899   Lefèvre, N., Moore, G., Aiken, J., Watson, A., and Cooper, D.: Variability of pCO2 in the
900   tropical Atlantic in 1995, J. Geophys. Res., C3, 5623-5634, https://doi.org/10.1029/97JC023031998.

901   Ljung, G. M., & Box, G. E.: On a measure of lack of fit in time series models. Biometrika,
902   65(2), 297-303, https://www.jstor.org/stable/2335207, 1978.

903   Locarnini R. A., Mishonov A. V., Antonov J. I., Boyer T. P., Garcia H. E., Baranova O. K.,
904   Zweng M. M., Paver C. R., Reagan J. R., Johnson D. R., Hamilton M., Seidov D.: World Ocean Atlas
905   2013, Volume 1: temperature. Levitus S, Ed.; Mishonov A, Technical Ed.; NOAA Atlas NESDIS 73,
906   40 pp, 2013.

907   Lopes dos Santos, R. A., Prange, M., Castañeda, I. S., Schefuß, E., Mulitza, S., Schulz, M.,
908   Niedermeyer, E. M., Sinninghe Damsté, J. S., and Schouten, S.: Glacial-interglacial variability in
909   Atlantic meridional overturning circulation and thermocline adjustments in the tropical North Atlantic,
910   Earth Planet. Sc. Lett., 300, 407-414, https://doi.org/10.1016/j.epsl.2010.10.030, 2010.

911   Lopes dos Santos, R. A. L., Spooner, M. I., Barrows, T. T., De Deckker, P., Sinninghe Damsté,
912   J. S., and Schouten, S.: Comparison of organic ($U^{K'}_{37}$, TEX_{86}^{H}, LDI) and faunal proxies (foraminiferal

913 assemblages) for reconstruction of late Quaternary sea surface temperature variability from offshore
914 southeastern Australia, Paleoceanography, 28, 377-387, https://doi.org/10.1002/palo.20035, 2013.

915 Lutjeharms, J. R. E.: The Agulhas Current, 330 pp., Springer, Berlin, 2006.

916 Malauene, B. S., Shillington, F. A., Roberts, M. J., and Moloney, C. L.: Cool, elevated
917 chlorophyll-a waters off northern Mozambique, Deep-Sea Res. Pt. II, 100, 68-78,
918 https://doi.org/10.1016/j.dsr2.2013.10.017, 2014.

919 Marlowe, I. T., Green, J. C., Neal, A. C., Brassell, S. C., Eglinton, G., and Course, P. A.: Long-
920 Chain (*n*-C$_{37}$–C$_{39}$) alkenones in the Prymnesiophyceae. Distribution of alkenones and other lipids and
921 their taxonomic significance, Brit. Phycol. J., 19, 203-216,
922 https://doi.org/10.1080/00071618400650221, 1984.

923 Martin, J. H., and Fitzwater, S. E.: Iron-deficiency limits phytoplankton growth in the Northeast
924 Pacific Subarctic, Nature, 331, 341-343, https://doi.org/10.1038/331341a0, 1988.

925 Mazeika, P. A.: Thermal domes in the Eastern Tropical Atlantic Ocean. Limnol. Oceanogr., 12,
926 537-539, https://doi.org/10.4319/lo.1967.12.3.0537, 1967.

927 Méjanelle, L., Sanchez-Gargallo, A., Bentaleb, I., and Grimalt, J. O.: Long chain *n*-alkyl diols,
928 hydroxy ketones and sterols in a marine eustigmatophyte, *Nannochloropsis gaditana*, and in *Brachionus*
929 *plicatilis* feeding on the algae, Org. Geochem., 34, 527-538, Pii s0146-6380(02)00246-2,
930 https://doi.org/10.1016/s0146-6380(02)00246-2, 2003.

931 Müller-Karger, F. E., McClain, C. R., and Richardson, P. L.: The dispersal of the Amazon´s
932 water, Nature, 333, 56-59, https://doi.org/10.1038/333056a0 1988.

933 Müller-Karger, F. E., Richardson, P. L., and McGillicuddy, D.: On the offshore dispersal of the
934 Amazon´s Plume in the North Atlantic: Comments on the paper by A. Longhurst, "Seasonal cooling and
935 blooming in tropical oceans", Deep-Sea Res. Pt. I, 42, 2127-2137, https://doi.org/10.1016/0967-
936 0637(95)00085-2, 1995.

937 Müller-Karger, F., Varela, R., Thunell, R., Scranton, M., Bohrer, R., Taylor, G., Capelo, J.,
938 Astor, Y., Tappa, E., Ho, T. Y., and Walsh, J. J.: Annual cycle of primary production in the Cariaco
939 Basin: Response to upwelling and implications for vertical export, J. Geophys. Res., 106, 4527-4542,
940 https://doi.org/10.1029/1999JC000291, 2001.

941 Müller-Karger, F., Varela, R., Thunell, R., Astor, Y., Zhang, H. Y., Luerssen, R., and Hu, C.
942 M.: Processes of coastal upwelling and carbon flux in the Cariaco Basin, Deep-Sea Res. Pt. II, 51, 927-
943 943, https://doi.org/10.1016/j.dsr2.2003.10.010, 2004.

944   Müller, P. J., Kirst, G., Ruhland, G., von Storch, I., and Rosell-Melé, A.: Calibration of the
945   alkenone paleotemperature index $U^{K'}_{37}$ based on core-tops from the eastern South Atlantic and the global
946   ocean (60°N-60°S), Geochim. Cosmochim. Ac., 62, 1757-1772, https://doi.org/10.1016/s0016-
947   7037(98)00097-0, 1998.

948   Müller, P. J., and Fischer, G.: A 4-year sediment trap record of alkenones from the filamentous
949   upwelling region off Cape Blanc, NW Africa and a comparison with distributions in underlying
950   sediments, Deep-Sea Res. Pt. I, 48, 1877-1903, https://doi.org/10.1016/S0967-0637(00)00109-6, 2001.

951   Naafs, B. D. A., Hefter, J., and Stein, R.: Application of the long chain diol index (LDI)
952   paleothermometer to the early Pleistocene (MIS 96), Org. Geochem., 49, 83-85,
953   http://doi.org/10.1016/j.orggeochem.2012.05.011, 2012.

954   NASA Aquarius project: Aquarius Official Release Level 3 Sea Surface Salinity Standard
955   Mapped Image Daily Data V4.0. Ver. 4.0. PO.DAAC, CA, USA, 2015a.

956   NASA Aquarius project: Aquarius Official Release Level 3 Wind Speed Standard Mapped
957   Image Daily Data V4.0. Ver. 4.0. PO.DAAC, CA, USA, 2015b.

958   Nehring, D., Hagen, E., Jorge da Silva, A., Schemainda, R., Wolf, G., Michelchen, N., Kaiser,
959   W., Postel, L., Gosselk, F., and Brenning, U.: The oceanological conditions in the western part of the
960   Mozambique Channel in February-March 1980, 1984.

961   Peeters, F. J. C., Acheson, R., Brummer, G. J. A., de Ruijter, W. P. M., Schneider, R. R.,
962   Ganssen, G. M., Ufkes, E., and Kroon, D.: Vigorous exchange between the Indian and Atlantic oceans
963   at the end of the past five glacial periods, Nature, 430, 661-665, http://doi.org/10.1038/nature02785,
964   2004.

965   Peterson, L. C., Overpeck, J. T., Kipp, N. G., and Imbrie, J.: A high-resolution Late Quaternary
966   upwelling record from the anoxic Cariaco Basin, Venezuela, Paleoceanography, 6, 99-119,
967   http://doi.org/10.1029/90pa02497, 1991.

968   Prahl, F. G., and Wakeham, S. G.: Calibration of unsaturation patterns in long-chain ketone
969   compositions for paleotemperature assessment, Nature, 330, 367-369, http://doi.org/10.1038/330367a0,
970   1987.

971   Prahl, F. G., Dymond, J., and Sparrow, M. A.: Annual biomarker record for export production
972   in the central Arabian Sea, Deep-Sea Res. II, 47, 1581-1604, https://doi.org/10.1016/S0967-
973   0645(99)00155-1, 2000.

974   Rampen, S. W., Schouten, S., Wakeham, S. G., and Sinninghe Damsté, J. S.: Seasonal and
975   spatial variation in the sources and fluxes of long chain diols and mid-chain hydroxy methyl alkanoates

976   in the Arabian Sea, Org. Geochem., 38, 165-179, https://doi.org/10.1016/j.orggepchem.2006.10.008,

977   2007.

978   Rampen, S. W., Schouten, S., Koning, E., Brummer, G.-J. A., and Sinninghe Damsté, J. S.: A

979   90 kyr upwelling record from the northwestern Indian Ocean using a novel long-chain diol index, Earth

980   Planet. Sc. Lett., 276, 207-213, https://doi.org/10.1016/j.epsl.2008.09.0222008.

981   Rampen, S. W., Schouten, S., and Sinninghe Damsté, J. S.: Occurrence of long chain 1,14-diols

982   in *Apedinella radians*, Org. Geochem., 42, 572-574, https://doi.org/10.1016/j.orggeochem.2011.03.009,

983   2011.

984   Rampen, S. W., Willmott, V., Kim, J. H., Uliana, E., Mollenhauer, G., Schefuss, E., Sinninghe

985   Damsté, J. S., and Schouten, S.: Long chain 1,13-and 1,15-diols as a potential proxy for

986   palaeotemperature   reconstruction,   Geochim.   Cosmochim.   Ac.,   84,   204-216,

987   https://doi.org/10.1016/j.gca.2012.01.024, 2012.

988   Rampen, S. W., Willmott, V., Kim, J. H., Rodrigo-Gámiz, M., Uliana, E., Mollenhauer, G.,

989   Schefuss, E., Sinninghe Damsté, J. S., and Schouten, S.: Evaluation of long chain 1,14-alkyl diols in

990   marine   sediments   as   indicators   for   upwelling   and   temperature,   Org.   Geochem.,   76,   39-47,

991   https://doi.org/10.1016/j.orggeochem.2014.07.012, 2014a.

992   Rampen, S. W., Datema, M., Rodrigo-Gámiz, M., Schouten, S., Reichart, G. J., and Sinninghe

993   Damsté, J. S.: Sources and proxy potential of long chain alkyl diols in lacustrine environments,

994   Geochim. Cosmochim. Ac., 144, 59-71, https://doi.org/10.1016/j.gca.2014.08.033, 2014b.

995   Reiche, S., Rampen, S. W., Dorhout, D. J. C., Sinninghe Damsté, J. S., and Schouten, S.: The

996   impact of oxygen exposure on long-chain alkyl diols and the long chain diol index (LDI) – a long-term

997   incubation study, Org. Geochem., 124, 238-246, https://doi.org/10.1016/j.orggeochem.2018.08.003,

998   2018.

999   Richards, F. A. 1975. The Cariaco Basin (Trench). Oceanogr. Mar. Biol. Ann. Rev. 13: 11–67.

1000   Richardson, P. L., and Reverdin, G.: Seasonal cycle of velocity in the Atlantic North Equatorial

1001   Countercurrent as measured by surface drifters, current meters, and ship drifts, J. Geophys. Res.-Oceans,

1002   92, 3691-3708, https://doi.org/10.1029/JC092iC04p03691, 1987.

1003   Ridderinkhof, H., van der Werf, P. M., Ullgren, J. E., van Aken, H. M., van Leeuwen, P. J., and

1004   de Ruijter, W. P. M.: Seasonal and interannual variability in the Mozambique Channel from moored

1005   current observations, J. Geophys. Res.-Oceans, 115, https://doi.org/10.1029/2009jc005619, 2010.

1006   Rodrigo-Gámiz, M., Rampen, S. W., de Haas, H., Baas, M., Schouten, S., and Sinninghe

1007   Damsté, J. S.: Constraints on the applicability of the organic temperature proxies $U^{K'}_{37}$, TEX_{86} and LDI

1008 in the subpolar region around Iceland, Biogeosciences, 12, 6573-6590, https://doi.org/10.5194/bg-12-
1009 6573-2015, 2015.

1010 Rodrigo-Gámiz, M., Rampen, S. W., Schouten, S., and Sinninghe Damsté, J. S.: The impact of
1011 oxic degradation on long chain alkyl diol distributions in Arabian Sea surface sediments, Org.
1012 Geochem., 100, 1-9, http://doi.org/10.1016/j.orggeochem.2016.07.003, 2016.

1013 Romero O. E., Lange C. B., Fischer G., Treppke U. F., Wefer G.: Variability in Export
1014 Production Documented by Downward Fluxes and Species Composition of Marine Planktic Diatoms:
1015 Observations from the Tropical and Equatorial Atlantic. In: Fischer G., Wefer G. (eds) Use of Proxies
1016 in Paleoceanography. Springer, Berlin, Heidelberg, 1999.

1017 Rosell-Melé, A., and Prahl, F. G.: Seasonality of $U^{K'}_{37}$ temperature estimates as inferred from
1018 sediment trap data, Quaternary Sci. Rev., 72, 128-136, https://doi.org/10.1016/j.quascirev.2013.04.017,
1019 2013.

1020 Rossignol, M., and A.M. Meyruis, Campagnes océanographiques du Gérard-Tréca, 53 pp.,
1021 Cent. Oceanogr. Dakar-Thiaroye, ORSTOM, Dakar, Senegal, 1964.

1022 Sætre, R., and Da Silva, A. J.: The circulation of the Mozambique channel, Deep Sea Res., 31,
1023 485-508, https://doi.org/10.1016/0198-0149(84)90098-0, 1984.

1024 Schlitzer, R.: Data Analysis and Visualization with Ocean Data View, CMOS Bulletin SCMO,
1025 43, 9–13, available at: https://odv.awi.de/, 2015.

1026 Schouten, M. W., de Ruijter, W. P. M., van Leeuwen, P. J., and Ridderinkhof, H.: Eddies and
1027 variability in the Mozambique Channel, Deep-Sea Res. Pt. II, 50, 1987-2003,
1028 https://doi.org/10.1016/s0967-0645(03)00042-0, 2003.

1029 Schouten, S., Hopmans, E. C., Schefuss, E., and Sinninghe Damsté, J. S.: Distributional
1030 variations in marine crenarchaeotal membrane lipids: a new tool for reconstructing ancient sea water
1031 temperatures?, Earth Planet. Sc. Lett., 204, 265-274, https://doi.org/10.1016/s0012-821x(02)00979-2,
1032 2002.

1033 Schouten, S., Hopmans, E. C., and Sinninghe Damsté, J. S.: The organic geochemistry of
1034 glycerol dialkyl glycerol tetraether lipids: A review, Org. Geochem., 54, 19-61,
1035 https://doi.org/10.1016/j.orggeochem.2012.09.006, 2013.

1036 Schreuder, L. T., Stuut, J.-B. W., Korte, L. F., Sinninghe Damsté, J. S., and Schouten, S.:
1037 Aeolian transport and deposition of plant wax *n*-alkanes across the tropical North Atlantic Ocean, Org.
1038 Geochem., 115, 113-123, https://doi.org/10.1016/j.orggeochem.2017.10.010, 2018a.

1039   Schreuder, L. T., Hopmans, E. C., Stuut, J.-B. W., Sinninghe Damsté, J. S., and Schouten, S.:
1040   Transport and deposition of the fire biomarker levoglucosan across the tropical North Atlantic Ocean,
1041   Geochim. Cosmochim. Ac., 227, 171-185, https://doi.org/10.1016/j.gca.2018.02.020, 2018b.

1042   Siedler, G., Zangenberg, N., and Onken, R.: Seasonal Changes in the Tropical Atlantic
1043   Circulation – Observation and Simulation of the Guinea Dome, J. Geophys. Res.-Oceans, 97, 703-715,
1044   https://doi.org/10.1029/91jc02501, 1992.

1045   Sinninghe Damsté, J. S., Rijpstra, W. I. C., Hopmans, E. C., Prahl, F. G., Wakeham, S. G., and
1046   Schouten, S.: Distribution of membrane lipids of planktonic Crenarchaeota in the Arabian seat, App.
1047   Environ. Micr., 68, 2997-3002, https://doi.org/10.1128/aem.68.6.2997-3002.2002, 2002.

1048   Sinninghe Damsté, J. S., Rijpstra, W. I. C., and Reichart, G.-J.: The influence of oxic
1049   degradation on the sedimentary biomarker record II. Evidence from Arabian Sea sediments, Geochim.
1050   Cosmochim. Ac., 66, 2737-2754, https://doi.org/10.1016/S0016-7037(02)00865-7, 2002.

1051   Sinninghe Damsté, J. S., Rampen, S., Rijpstra, W. I. C., Abbas, B., Muyzer, G., and Schouten,
1052   S.: A diatomaceous origin for long-chain diols and mid-chain hydroxy methyl alkanoates widely
1053   occurring in Quaternary marine sediments: Indicators for high-nutrient conditions, Geochim.
1054   Cosmochim. Ac., 67, 1339-1348, https://doi.org/10.1016/s0016-7037(02)01225-5 2003.

1055   Sinninghe Damsté, J. S., Rijpstra, W. I. C., Hopmans, E. C., den Uijl, M. J., Weijers, J. W. H.,
1056   and Schouten, S.: The enigmatic structure of the crenarchaeol isomer, Org. Geochem., 124, 22-28,
1057   https://doi.org/10.1016/j.orggeochem.2018.06.005, 2018.

1058   Smith, S. L.: Understanding the Arabian Sea: Reflections on the 1994-1996 Arabian Sea
1059   Expedition, Deep-Sea Res. Pt. II, 48, 1385-1402, https://doi.org/10.1016/S0967-0645(00)00144-2,
1060   2001.

1061   Stramma, L., and Schott, F.: The mean flow field of the tropical Atlantic Ocean, Deep-Sea Res.
1062   Pt. II, 46, 279-303, https://doi.org/10.1016/s0967-0645(98)00109-x, 1999.

1063   Stuut, J.-B., Zabel, M., Ratmeyer, V., Helmke, P., Schefuß, E., Lavik, G., and Schneider, R.:
1064   Provenance of present-day eolian dust collected off NW Africa, J. .Geophys. Res.-Atmos., 110, D04202-
1065   04201-D04202-04214, https://doi.org/10.1029/2004JD005161, 2005.

1066   Thunell, R. C., Varela, R., Llano, M., Collister, J., Müller-Karger, F., and Bohrer, R.: Organic
1067   carbon fluxes, degradation, and accumulation in an anoxic basin: Sediment trap results from the Cariaco
1068   Basin, Limnol. Oceanogr., 45, 300-308, https://doi.org/10.4319/lo.2000.45.2.0300, 2000.

1069   Thunell, R., Benitez-Nelson, C., Varela, R., Astor, Y., and Müller-Karger, F.: Particulate
1070   organic carbon fluxes along upwelling-dominated continental margins: Rates and mechanisms, Global
1071   Biogeochem. Cy., 21, https://doi.org/10.1029/2006gb002793, 2007.

1072   Tierney, J. E.: 12.14 - Biomarker-Based Inferences of Past Climate: The TEX_{86}
1073   Paleotemperature Proxy A2 - Holland, Heinrich D, in: Treatise on Geochemistry (Second Edition),
1074   edited by: Turekian, K. K., Elsevier, Oxford, 379-393, 2014.

1075   Tierney, J. E., and Tingley, M. P.: A Bayesian, spatially-varying calibration model for the TEX_{86}
1076   proxy, Geochim. Cosmochim. Ac., 127, 83-106, https://doi.org/10.1016/j.gca.2013.11.026, 2014.

1077   Tierney, J. E., and Tingley, M. P.: A TEX_{86} surface sediment database and extended Bayesian
1078   calibration, Scientific Data, 2, 150029, https://doi.org/10.1038/sdata.2015.29, 2015.

1079   Tierney, J. E., Sinninghe Damsté, J. S., Pancost, R. D., Sluijs, A., and Zachos, J. C.: Eocene
1080   temperature gradients, Nature Geosci, 10, 538-539, https://doi.org/10.1038/ngeo2997, 2017

1081   Tierney, J. E., and Tingley, M. P.: BAYSPLINE: A New Calibration for the Alkenone
1082   Paleothermometer, Paleoceanography and Paleoclimatology, 33, 281-301,
1083   https://doi.org/10.1002/2017pa003201, 2018.

1084   Torrence, C., Compo, G. P.: A practical guide to wavelet analysis. Bull. Am. Meteorol. Soc.79,
1085   61–78, https://doi.org/10.1175/1520-0477(1998)079<0061:APGTWA>2.0.CO;2, 1998.

1086   Treppke, U. F., Lange, C. B., and Wefer, G.: Vertical fluxes of diatoms and silicoflagellates in
1087   the eastern equatorial Atlantic, and their contribution to the sedimentary record, Mar. Micropaleontol.,
1088   28, 73-96, https://doi.org/10.1016/0377-8398(95)00046-1, 1996.

1089   Turich, C., Schouten, S., Thunell, R. C., Varela, R., Astor, Y., and Wakeham, S. G.: Comparison
1090   of TEX_{86} and $U^{K'}_{37}$ temperature proxies in sinking particles in the Cariaco Basin, Deep-Sea Res. Pt. I,
1091   78, 115-133, http://doi.org/10.1016/j.dsr.2013.02.008, 2013.

1092   Ullgren, J. E., van Aken, H. M., Ridderinkhof, H. and de Ruijter, W. P. M.: The hydrography
1093   of the Mozambique Channel from six years of continuous temperature, salinity, and velocity
1094   observations. Deep-Sea Res. Pt. I, 69, 36 – 50, https://doi.org/10.1016/j.dsr.2012.07.003, 2012.

1095   Villanueva, L., Besseling, M., Rodrigo-Gámiz, M., Rampen, S. W., Verschuren, D., and
1096   Sinninghe Damsté, J. S.: Potential biological sources of long chain alkyl diols in a lacustrine system,
1097   Org. Geochem., 68, 27-30, https://doi.org/10.1016/j.orggeochem.2014.01.001, 2014.

1098   van der Does, M., Korte, L. F., Munday, C. I., Brummer, G. J. A., and Stuut, J. B. W.: Particle
1099   size traces modern Saharan dust transport and deposition across the equatorial North Atlantic, Atmos.
1100   Chemis. Phys., 16, 13697-13710, https://doi.org/10.5194/acp-16-13697-2016, 2016.

1101   Versteegh, G. J. M., Bosch, H. J., and de Leeuw, J. W.: Potential palaeoenvironmental
1102   information of C_{24} to C_{36} mid-chain diols, keto-ols and mid-chain hydroxy fatty acids; a critical review,
1103   Org. Geochem., 27, 1-13, https://doi.org/10.1016/s0146-6380(97)00063-6, 1997.

1104   Versteegh, G. J. M., Jansen, J. H. F., de Leeuw, J. W., and Schneider, R. R.: Mid-chain diols
1105   and keto-ols in SE Atlantic sediments: a new tool for tracing past sea surface water masses?, Geochim.
1106   Cosmochim. Ac., 64, 1879-1892, https://doi.org/10.1016/S0016-7037(99)00398-1, 2000.

1107   Voituriez, B.: Les sous-courants 6quatoriaux nord et sud et la formation des dômes thermiques
1108   tropicaux, Oceanol. Acta, 4,497-506, 1981.

1109   Volkman, J. K., Eglinton, G., Corner, E. D. S., and Sargent, J. R.: Novel unsaturated straight-
1110   chain C_{37}-C_{39} methyl and ethyl ketones in marine sediments and a coccolithophore *Emiliania huxleyi*,
1111   Phys. Chem. Earth, 12, 219-227, http://doi.org/10.1016/0079-1946(79)90106-X, 1980.

1112   Volkman, J. K., Barrett, S. M., Dunstan, G. A., and Jeffrey, S. W.: C_{30}–C_{32} alky diols and
1113   unsaturated alcohols in microalgae of the class Eustigmatophyceae, Org. Geochem., 18, 131-138,
1114   http://doi.org/10.1016/0146-6380(92)90150-v, 1992.

1115   Volkman, J. K., Barrett, S. M., Blackburn, S. I., and Sikes, E. L.: Alkenones in *Gephyrocapsa*
1116   *Oceanica* – Implications for studies of paleoclimate, Geochim. Cosmochim. Ac., 59, 513-520,
1117   http://doi.org/10.1016/0016-7037(95)00325-t, 1995.

1118   Volkman, J. K., Barrett, S. M., and Blackburn, S. I.: Eustigmatophyte microalgae are potential
1119   sources of C_{29} sterols, C_{22}–C_{28} *n*-alcohols and C_{28}–C_{32} *n*-alkyl diols in freshwater environments, Org.
1120   Geochem., 30, 307-318, http://doi.org/10.1016/s0146-6380(99)00009-1, 1999.

1121   Wakeham, S. G., Peterson, M. L., Hedges, J. I., and Lee, C.: Lipid biomarker fluxes in the
1122   Arabian Sea, with a comparison to the equatorial Pacific Ocean, Deep-Sea Res. Pt. II, 49, 2265-2301,
1123   https://doi.org/10.1016/S0967-0645(02)00037-1, 2002.

1124   Warnock, J. P., Bauersachs, T., Kotthoff, U., Brandt, H. T., and Andren, E.: Holocene
1125   environmental history of the Angermanalven Estuary, northern Baltic Sea, Boreas, 47, 593-608,
1126   https://doi.org/10.1111/bor.12281, 2018.

1127   Weijer, W., de Ruiter, W. P. M., Dijkstra, H. A., and van Leeuwen, P. J.: Impact of interbasin
1128   exchange on the Atlantic overturning circulation, J. Phys. Oceanogr., 29, 2266-2284,
1129   https://doi.org/10.1175/1520-0485(1999)029<2266:Ioieot>2.0.Co;2, 1999.

1130   Willmott, V., Rampen, S. W., Domack, E., Canals, M., Sinninghe Damsté, J. S., and Schouten,
1131   S.: Holocene changes in Proboscia diatom productivity in shelf waters of the north-western Antarctic
1132   Peninsula, Antarct. Sci., 22, 3-10, https://doi.org/10.1017/s095410200999037x, 2010.

1133   Wuchter, C., Schouten, S., Wakeham, S. G., and Sinninghe Damsté, J. S.: Temporal and spatial
1134   variation in tetraether membrane lipids of marine Crenarchaeota in particulate organic matter:
1135   Implications   for TEX_{86} paleothermometry,   Paleoceanography,   20,
1136   https://doi.org/10.1029/2004pa001110, 2005.

1137   Wuchter, C., Schouten, S., Wakeham, S. G., and Sinninghe Damsté, J. S.: Archaeal tetraether
1138   membrane lipid fluxes in the northeastern Pacific and the Arabian Sea: Implications for TEX_{86}
1139   paleothermometry,   Paleoceanography,   21,   PA4208-4201-PA4208-4209,
1140   https://doi.org/10.1029/2006PA001279, 2006.

1141   Xie, P. and Arkin, P.A.: Global precipitation: A 17-year monthly analysis based on gauge
1142   observations, satellite estimates, and numerical model outputs. Bull. Am. Meteor. Soc., 78, 2539 – 2558,
1143   https://doi.org/10.1175/1520-0477(1997)078<2539:GPAYMA>2.0.CO;2, 1997.

1144   Yamagata, T., and Iizuka, S.: Simulation of the Tropical Thermal Domes in the Atlantic – A
1145   Seasonal   Cycle,   J.   Phys.   Oceanogr.,   25,   2129-2140,   https://doi.org/10.1175/1520-
1146   0485(1995)025<2129:Sotttd>2.0.Co;2, 1995.

1147   Yamamoto, M., Shimamoto, A., Fukuhara, T., Tanaka, Y., and Ishizaka, J.: Glycerol dialkyl
1148   glycerol tetraethers and TEX_{86} index in sinking particles in the western North Pacific, Org. Geochem.,
1149   53, 52-62, https://doi.org/10.1016/j.orggeochem.2012.04.010, 2012.

1150   Zhang, Y. G., and Liu, X. Q.: Export Depth of the TEX_{86} Signal, Paleoceanography and
1151   Paleoclimatology, 33, 666-671, https://doi.org/10.1029/2018PA003337, 2018.

1152
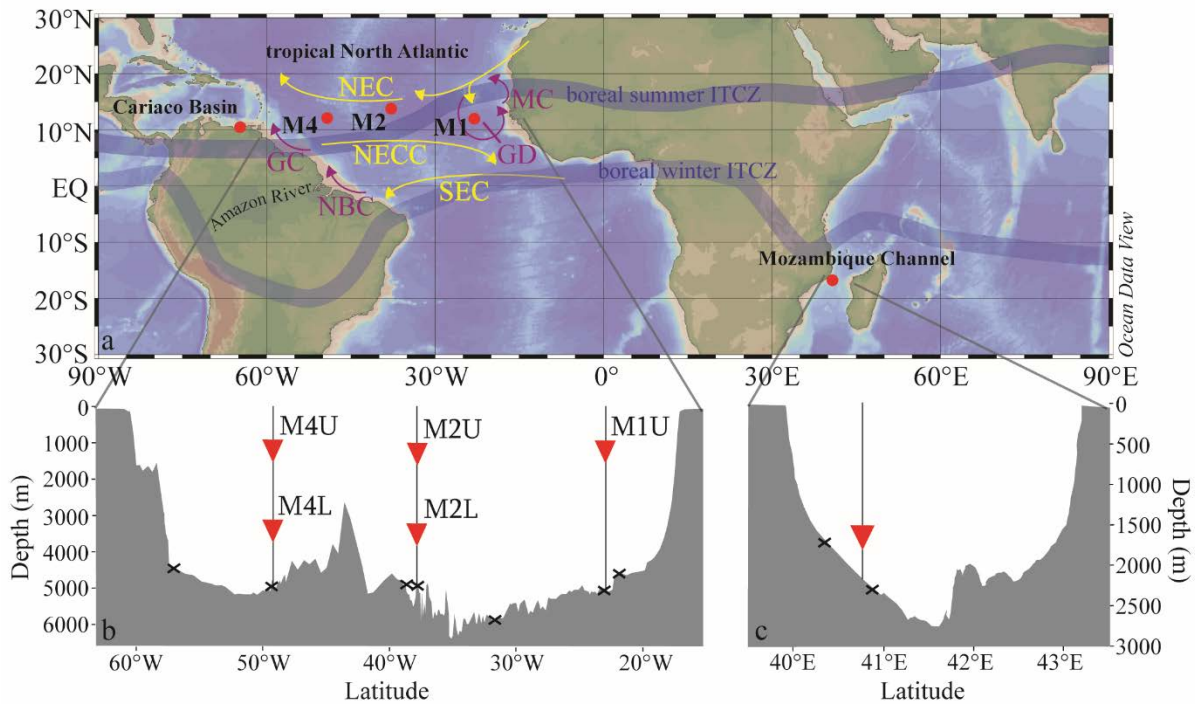
1153

Fig. 1 **(a)** Location map showing the five sediment trap mooring sites in the Cariaco Basin, the tropical North Atlantic (M1, M2 and M4) and the Mozambique Channel. Two of the moorings in the tropical North Atlantic (M2 and M4) contain an upper ('U') and a lower ('L') trap, shown in the bathymetric section below **(b)** with traps depicted as red triangles and surface sediments shown as black crosses. A similar section profile is shown for the Mozambique Channel (c), where also the sediment trap and the surface sediments are indicated. All maps/sections are generated in Ocean Data View (Schlitzer, 2015). Indicated are the approximate seasonal positions of the ITCZ. NEC = North Equatorial Current; NECC = North Equatorial Countercurrent; SEC = South Equatorial Current; MC = Mauritania Current; GD = Guinea Dome; NBC = North Brazil Current; GC = Guiana Current.
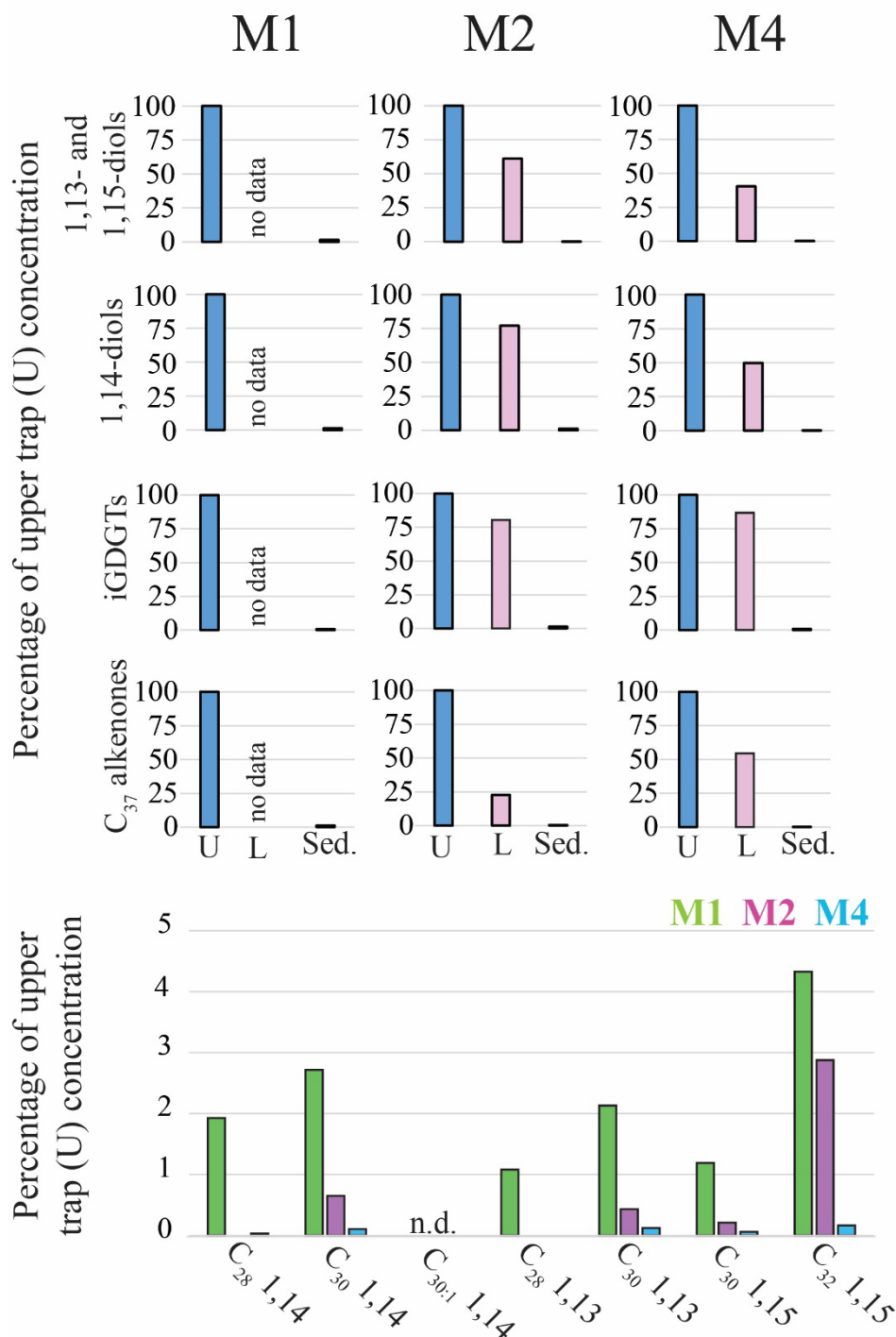
1163

Fig. 2 Relative concentrations of biomarker lipids for the mooring sites M1, M2 and M4 in the tropical North Atlantic. Upper panel: percentages of lipid biomarkers in the lower traps ('L'; 3500 m) and the surface sediments ('Sed.') relative to the annual flux-weighted concentrations in the upper traps ('U'; 1200 m; set at 100%). The lower panel shows the preservation of the individual LCDs (sediments versus upper trap flux-weighted concentration) for the three sediment trap sites. For M1 and M2 the sedimentary LCD concentrations were based on the average of the two nearby underlying surface sediments (Fig. 1). When no bar is shown then the LCD was not detected.
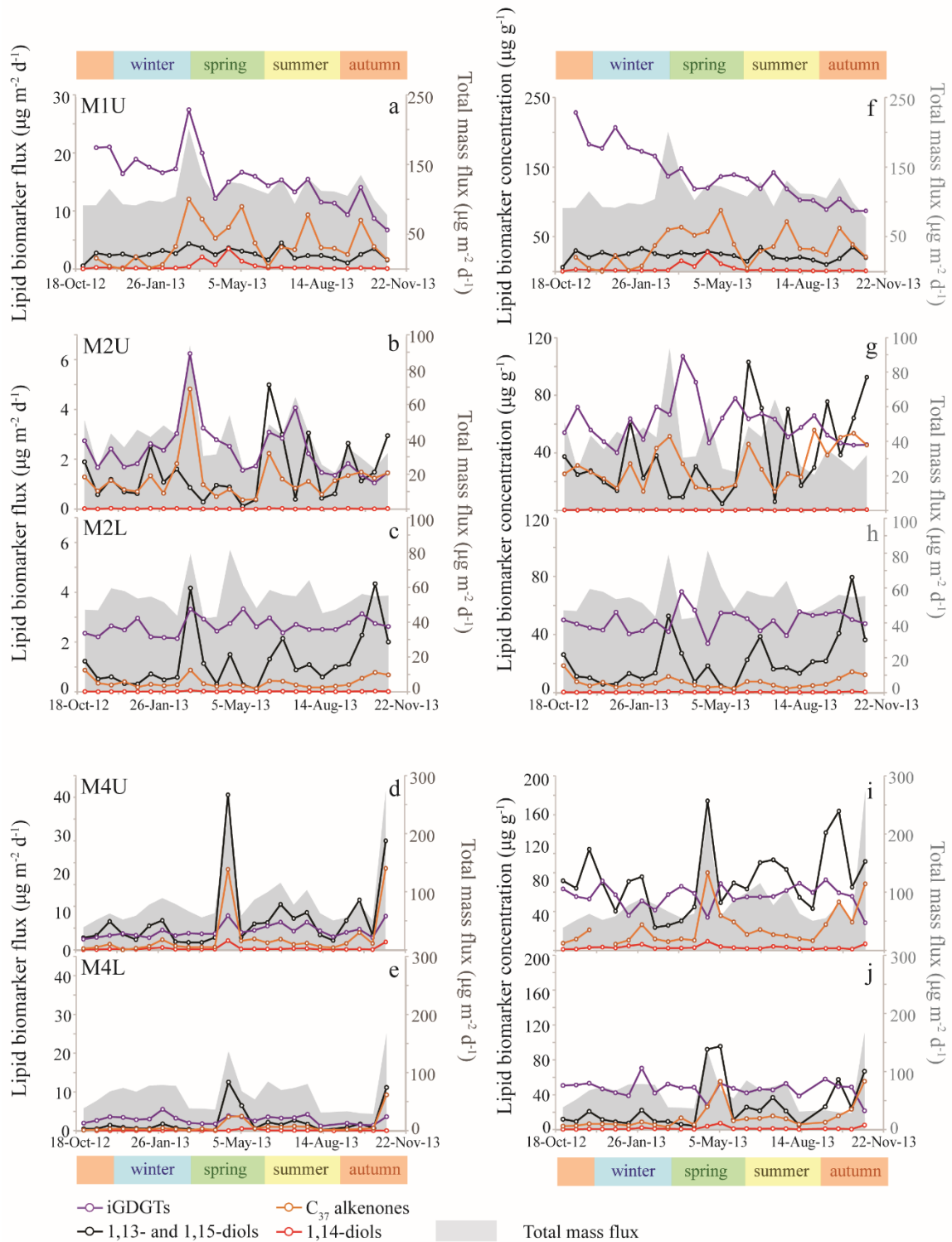
Fig. 3 Lipid biomarker fluxes for the tropical North Atlantic sediment traps, i.e., M1, upper and lower M2, and upper and lower M4 in panels **(a)** to **(e)**. Lipid biomarker fluxes (iGDGTs in purple; C_{37} alkenones in orange; 1,13- and 1,15-diols in black; 1,14-diols in red) are indicated on the left *y*-axis, and the total mass flux (grey stack; Korte et al., 2017) on the right *y*-axis. Lipid biomarker concentrations are plotted in panels **(f)** to **(j)**, with biomarker concentrations on the left *y*-axis, and the total mass flux on the right *y*-axis. Note that the *y*-axes are different per sediment trap site, but identical for upper (U) and lower (L) traps.
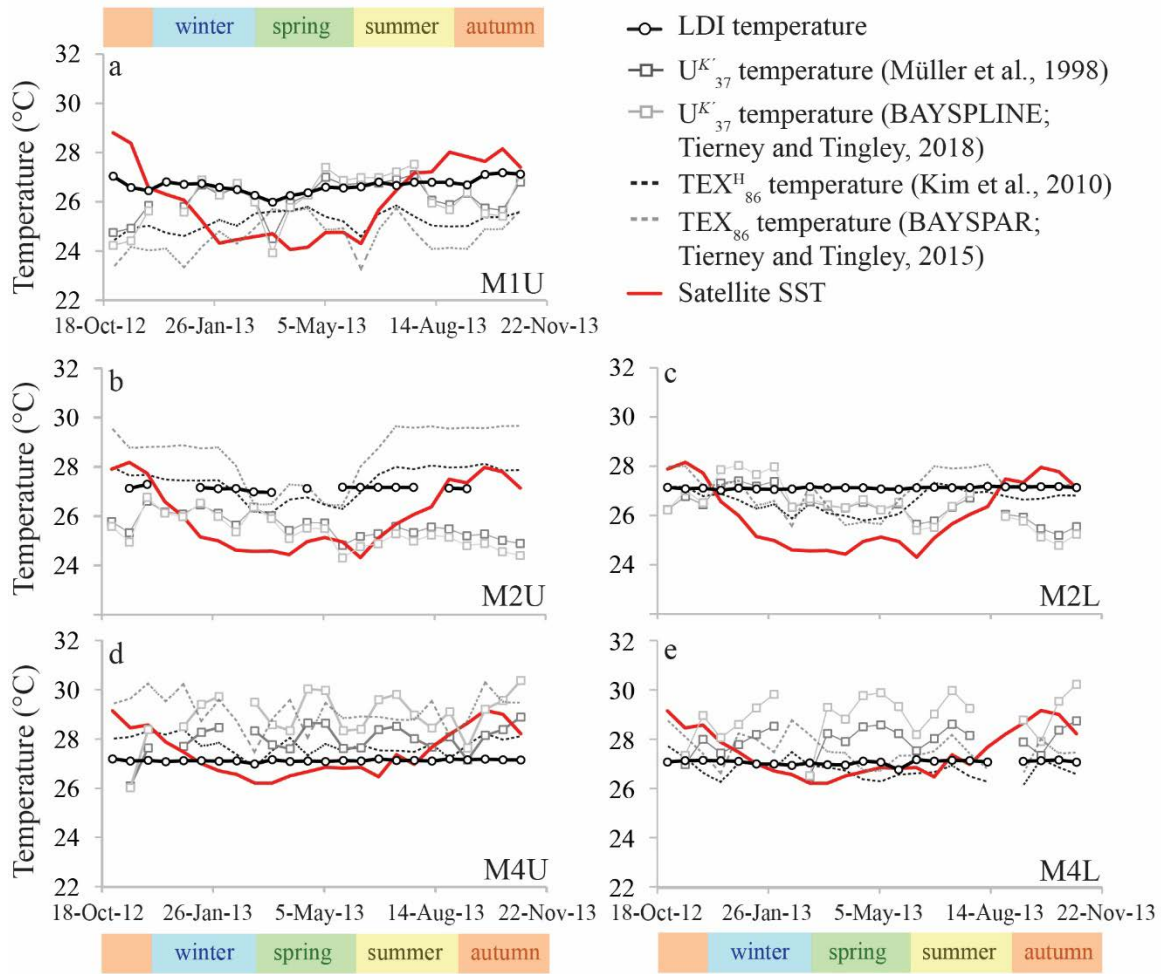
1178

1179 **Fig. 4** Temperature proxy records for the tropical North Atlantic. Panel **(a)** shows upper trap station

1180 M1, **(b)** upper trap station M2 and **(c)** lower trap M2, respectively, **(d)** upper trap station M4 and **(e)**

1181 lower trap station M4, respectively.

1182
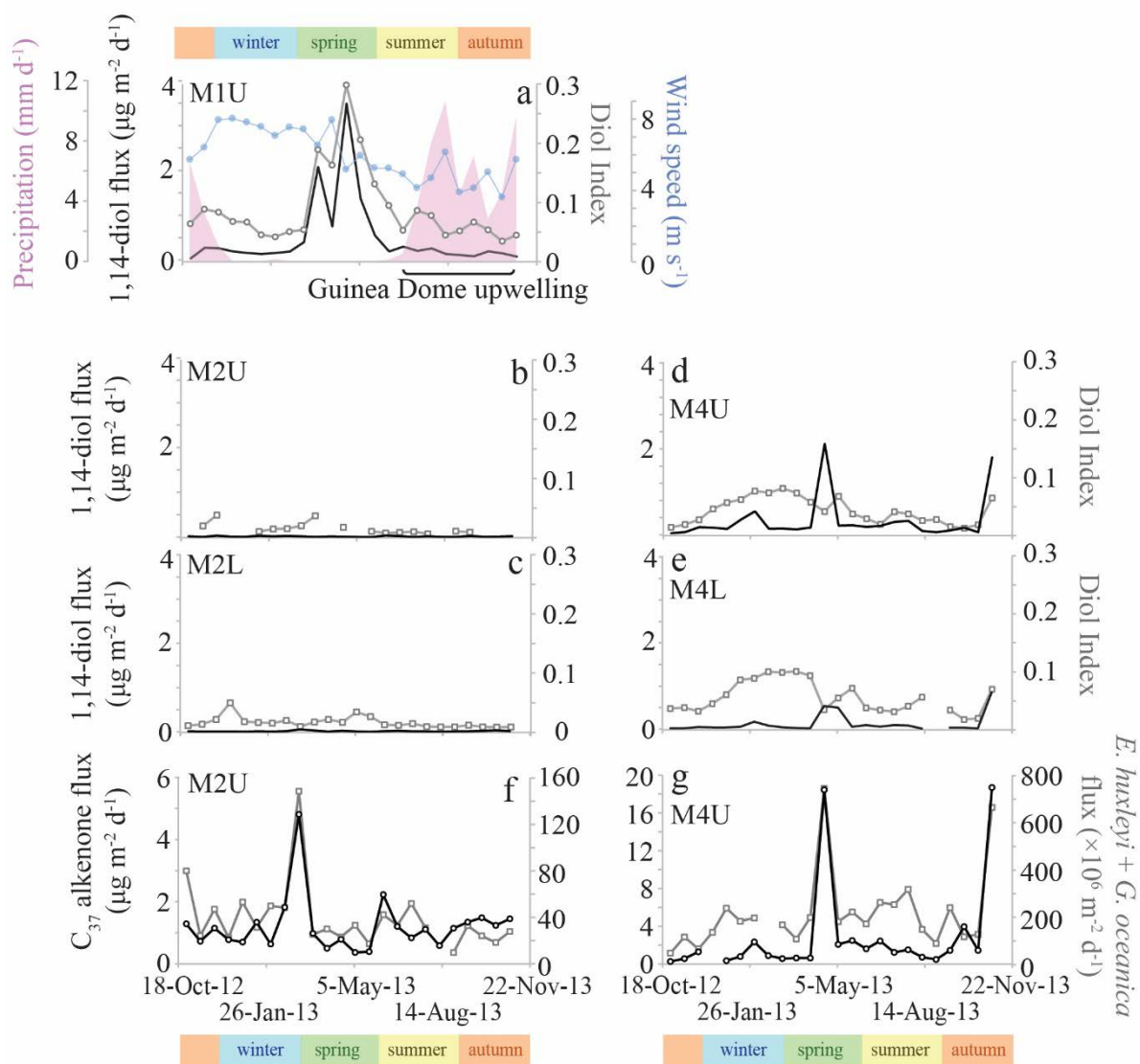
1183

Fig. 5 Phytoplankton productivity records for the tropical North Atlantic. Panels **(a)** – **(e)** show the 1,14-diol fluxes (left *y*-axis; black) and the Diol Index (right *y*-axis; grey) for sediment traps. The *y*-axes are the same for these panels. Wind speed and precipitation data were adapted from Guerreiro et al. (in revision); for references regarding remote sensing parameters, see Guerreiro et al. (2017). Panels **(f)** and **(g)** show the C_{37} alkenone fluxes (left *y*-axis; black) and combined fluxes of *E. huxleyi* and *G. oceanica* (from Guerreiro et al., 2017; right *y*-axis; grey) for the upper traps of M2 and M4.

1190

1191

1192

1193

1194
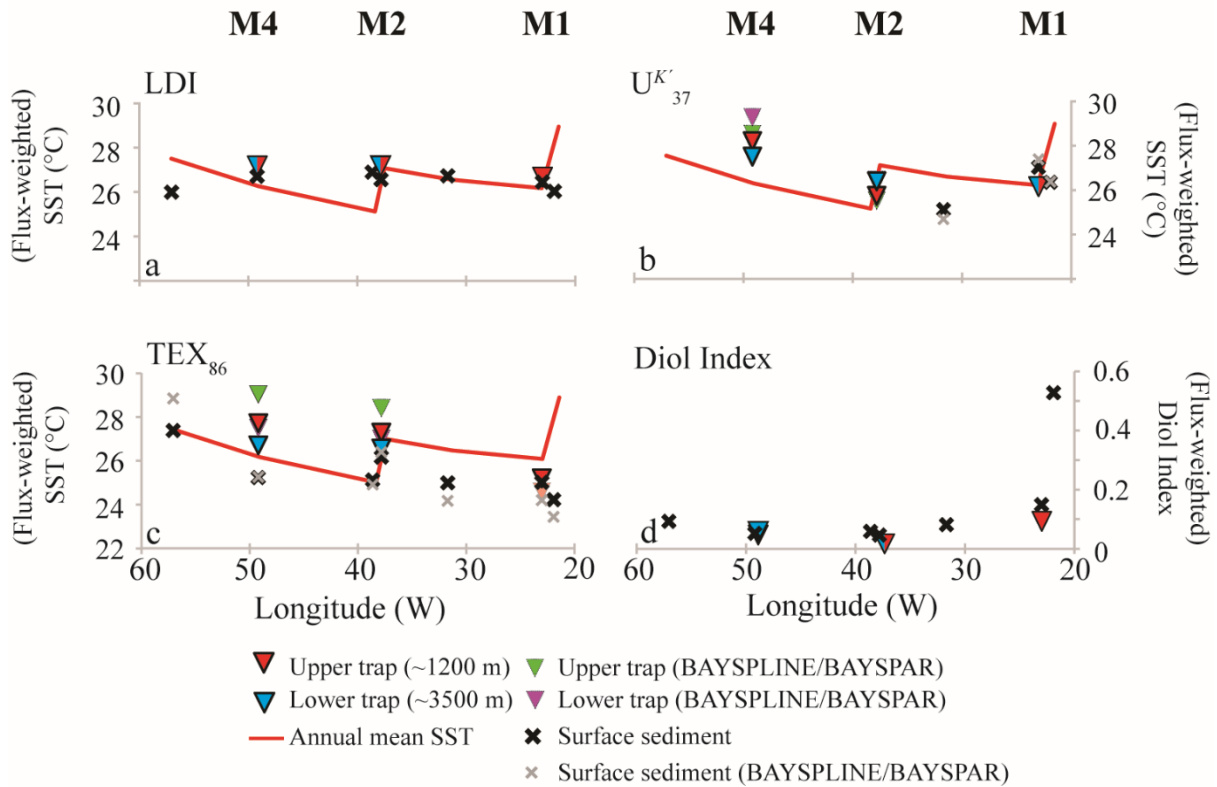
1195

1196 **Fig. 6** Flux-weighted average (annual) proxy results for the sediment traps compared with the underlying

1197 sediments (crosses) and annual mean SST (red line; specific for coordinates of the surface sediments;

1198 World Ocean Atlas 2013 ¼ grid resolution). Panel **(a)**, **(b)** and **(c)** show the LDI, $U^{K'}_{37}$ and TEX_{86}

1199 temperature results, respectively. Triangles reflect sediment trap results (red = upper/~1200 m; blue =

1200 lower/~3500 m), and crosses represent surface sediments. In case of the $U^{K'}_{37}$ and TEX_{86}, the green and

1201 purple triangles and grey crosses reflect the temperatures calculated using the BAYSPLINE and

1202 BAYSPAR models (Tierney and Tingley, 2014; 2015; 2018), whereas the other temperatures were

1203 calculated by means of the Müller et al. (1998) and Kim et al. (2010; TEX^{H}_{86}) calibrations, respectively.

1204 Panel **(d)** shows the flux-weighted average Diol Index values for the sediment traps, and the Diol Index

1205 estimates for the surface sediments.

1206

1207

1208

1209

1210
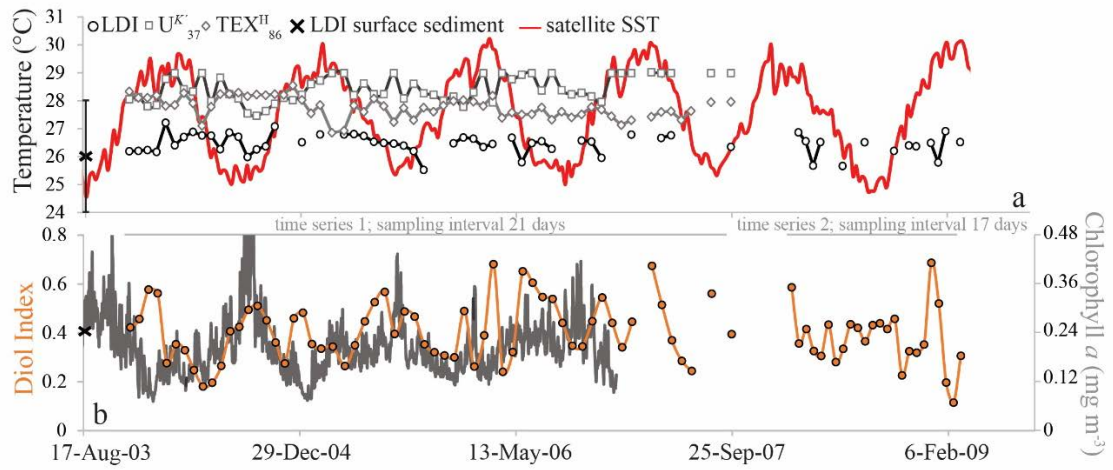
1211

Fig. 7 The LDI-derived temperatures, together with the TEX$^H_{86}$ and U$^{K'}_{37}$-derived temperatures and satellite SST (Fallet et al., 2011) (**a**) and the Diol Index (**b**) for the Mozambique Channel sediment trap. The black cross in panel (**a**) reflects the average LDI temperature of two underlying surface sediments, with the LDI calibration error. The chlorophyll *a* data is from Fallet et al. (2011).

1216

1217
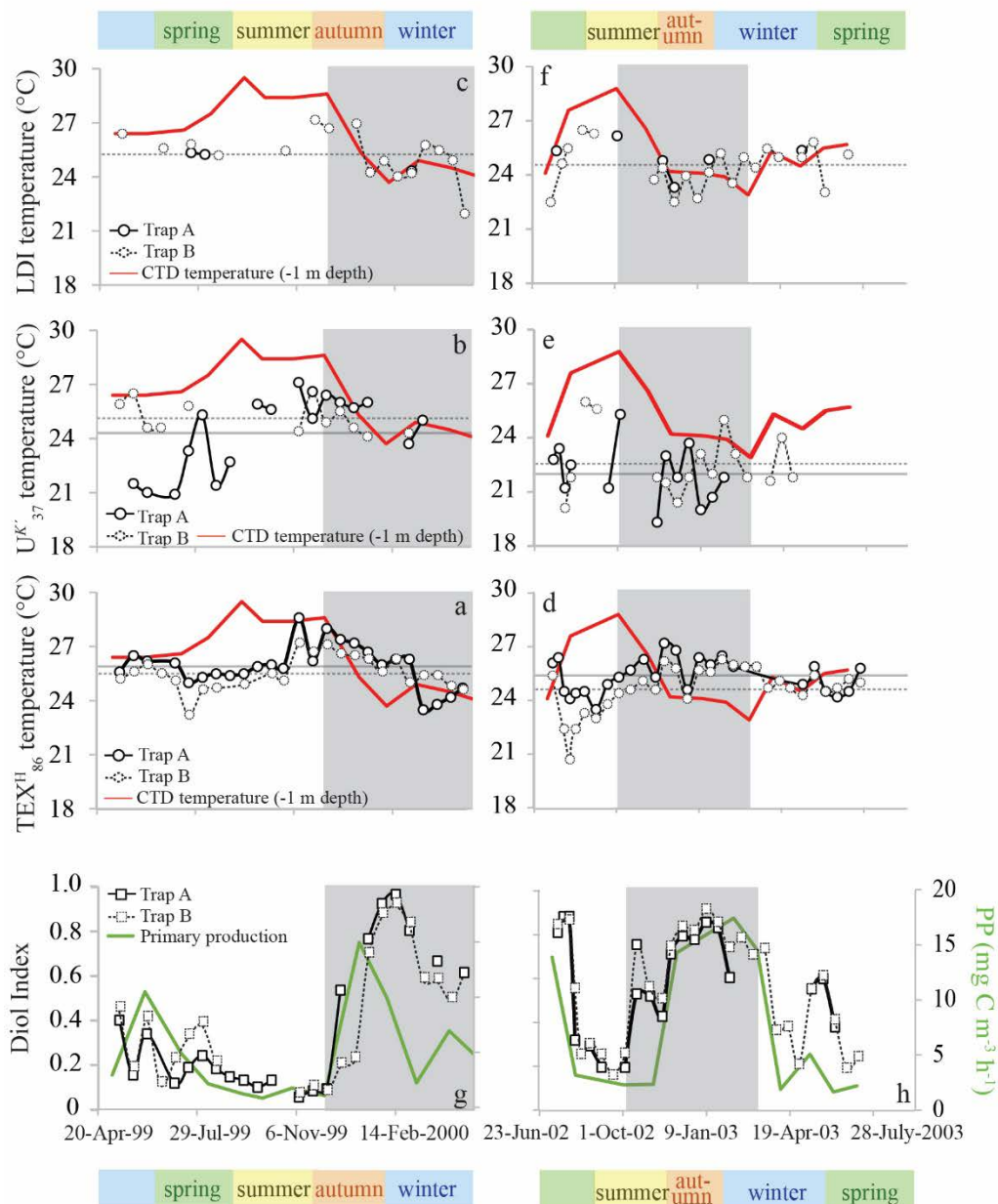
Fig. 8 Seasonal proxy derived temperature and upwelling/productivity records for the sediment traps in the Cariaco Basin. Panels **(a)**, **(b)** and **(c)** show the May 1999 – May 2000 time series TEX$^H_{86}$-, U$^{K'}_{37}$- and LDI-derived temperature reconstructions for Trap A (275 m depth; solid symbols) and Trap B (455 m depth; dashed symbols), respectively. Panels **(d)**, **(e)** and **(f)** show the proxy data for the July 2002 – July 2003 time series, with CTD-temperatures (1 m depth) in red. The U$^{K'}_{37}$, TEX$^H_{86}$ and CTD temperatures are adopted from Turich et al. (2013). The horizontal lines reflect the average proxy-derived temperatures (Trap A = solid; Trap B = dashed). Panel **(g)** and **(h)** show the 1,14-diol based Diol Index (Rampen et al., 2008) for the 1999-2000 and 2002-2003 time series, respectively, for Trap A (275 m depth; solid symbols) and Trap B (455 m depth; dashed symbols). Primary productivity in mg C m^{-3} h^{-1} is plotted in green (data adopted from Turich et al., 2013). The shaded area reflects the period of upwelling.

1230

1231

1232

1233

1234

1235

1236
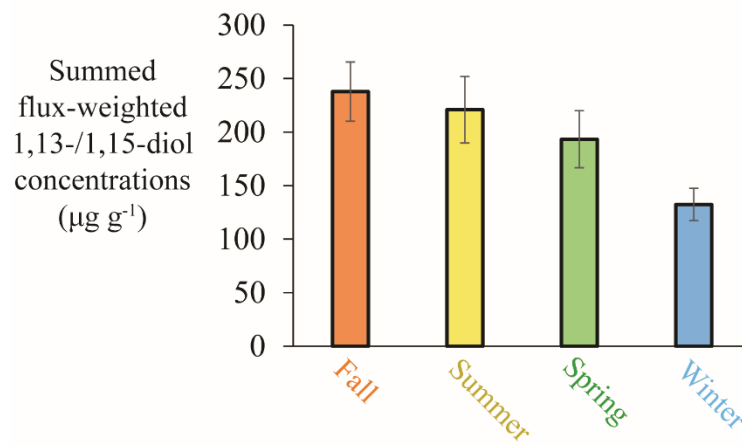
1237 **Fig. 9** Seasonal summed flux-weighted average of 1,13-/1,15-diol concentrations in all sediment traps

1238 (station M1 upper trap, station M2 upper and lower trap and station M4 upper and lower trap) of the

1239 tropical North Atlantic.

1240
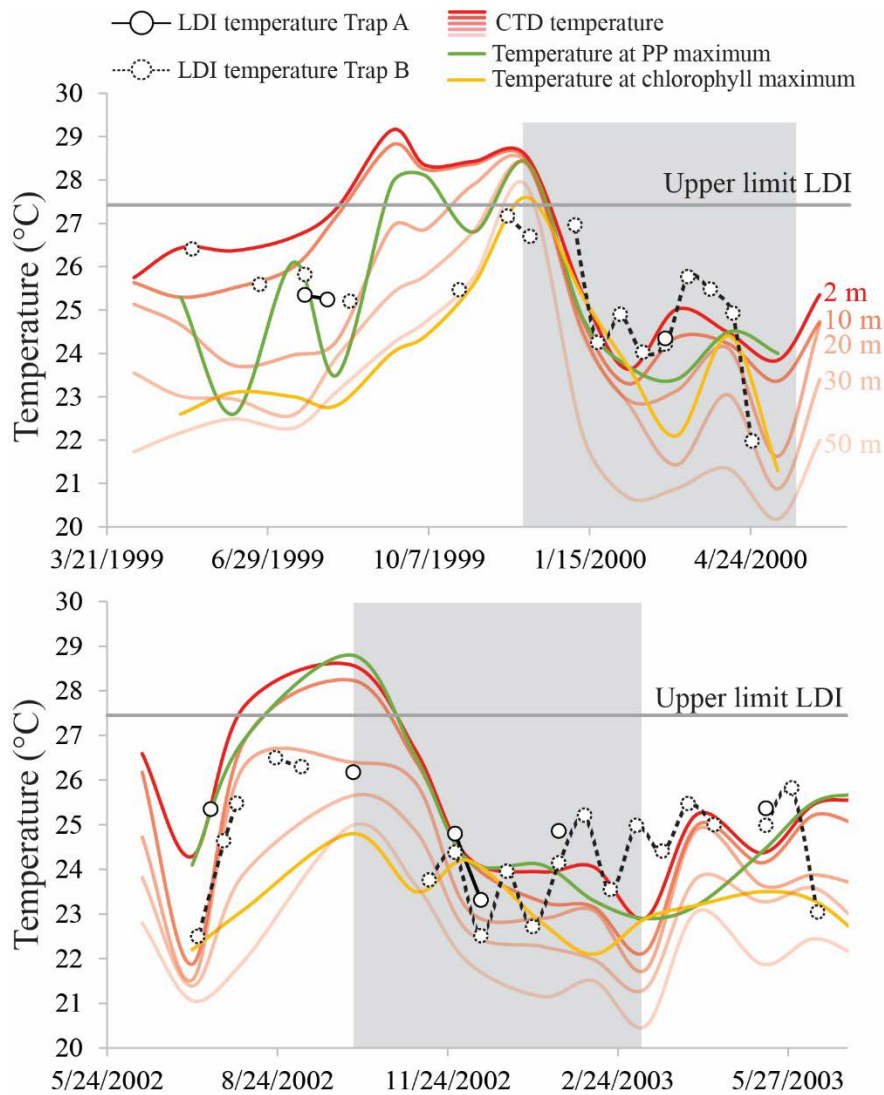
1241

1242 **Fig. 10** LDI temperature records for the Cariaco Basin time series May 1991 – May 2000 and July 2002

1243 – July 2003 for Trap A (275 m depth; solid symbols) and Trap B (455 m depth; dashed symbols), with

1244 CTD-derived temperatures at 2, 10, 20, 30 and 50 m depth (in red;

1245 http://www.imars.usf.edu/CAR/index.html; CARIACO time series composite CTD profiles), the

1246 temperature at the depth of maximum primary production (green) and the temperature at the depth of

1247 the chlorophyll maximum (yellow; data adapted from Turich et al., 2013). The shaded area represents

1248 the upwelling season.

1249